Electrochemical Performance of Si-based Material / C Composite Anode for Lithium-ion Batteries

March 2012

Qin Si

Introduction

There has been an endless demand of the high energy density of the battery toward a long time operation for the functional expansion of the notebook PC and a smart phone for IT. The energy density of the widely used Li-ion batteries with the graphite anode and the $LiCoO_2$ cathode has been improved in the past several decades. Compared to conventional aqueous rechargeable cells, such as nickel–cadmium and nickel metal hydride, Li-ion batteries have higher energy density, higher operating voltages, lower self-discharge, and lower maintenance requirements [1]. However, the current graphite anode has attained the theoretical capacity practically, and further improvement in energy density is actually impossible as far as the conventional cell chemistries are concerned. Recent attention paid to electric vehicle (EV) with respect to improvements in mileage also requires higher energy density for Li-ion batteries.

In 1971, Dey [2] reported that lithium can be electrochemically alloyed with a number of metals at room temperature, including Sn, Pb, Al, Au, Pt, Zn, Cd, Ag, and Mg. However, the alloying process resulted in complete disintegration of the electrodes and loss of electronic contact. Similarly, Sharma and Seefurth [3] reported the formation of Li-Si alloys in high temperature cells operating in the 400-500 ºC range. It was described that the alloying proceeded stepwise as formation of $Li_{12}Si_7$, $Li_{14}Si_6$, $Li_{13}Si_4$, and $Li_{22}Si_5$ alloys. Study of the Li-Si binary system [3, 4] indicated that each silicon atom can accommodate 4.4 lithium atoms at most, that is to say $Li_{22}Si_5$ alloy. The specific insertion capacity is 4200 mAh g^{-1}, which is the highest among the above alloying elements, and low Li-insertion potential versus Li/Li^+. In addition to its outstanding advantages, silicon is the second most abundant element on the earth.

Because of these attributes, a great deal of attention has been paid to silicon as a Li-ion battery anode material. However, large volume changes which take place during Li-insertion and extraction was intrinsic and serious issue, which causes pulverization or crumbling of the active materials followed by a loss of electrical contact. As a result, the Si electrode shows a rapid capacity fade during cycling [4].

To cope with the Si issue mechanical countermeasures to lessen as absorb the stress caused by the volume changes showed be key technologies. There are two strategies to improve the silicon-base electrode: one is to decrease the scale of active Si domain to nanoscale, the other is to fabricate the composite structures, including new binders, electrolyte additives and current collectors.

1 Reducing Si particle size to nanometer range

Nano-technology can be divided into zero-dimensional, one-dimensional and two-dimensional technology. Zero-dimensional nano-technology can be used to prepare nanometer silicon powder [5, 6]. By decreasing the particle size to nanometer-scale, controlling the volume change, and short the lithium ion diffusion distance to improve the electrochemical reaction rate. While, when the size down to below 100nm, silicon active particles is very easy to reunion during the Li-insertion and extraction to form the electrochemical sintering [7], contrary accelerated the capacity decay. Moreover, nanometer silicon powder shows a large surface area, increases in direct contact with the electrolyte led to a large irreversible capacity and reduces the coulomb efficiency. In addition, nanometer silicon powder produced mainly by the laser method, preparation costs are very high.

One-dimensional nano-technology can be used to prepare silicon nanowire and

silicon nanotube [8-11]. Silicon nanowires can reduce the volume change on the radial direction during the Li-insertion and extraction to achieve good cycle stability, and in the axial direction to provide rapid transfer of lithium ion [12]. But, in general, single-dimensional silicon nano material is not obvious advantages to compare nano particles, and because of the production cost is high, production cycle is long, and nanowires length is finite, it is difficult to practicality.

Two-dimensional nano-technology can be used to prepare silicon films [13]. Thinning can reduce the vertical direction volume change, thus maintain the structural integrity of the electrode. A most roughened surface could be obtained by depositing electrolytically on a copper foil and the surface revealed a jammed group of tiny pyramid like steeple-crowned caps. A 3.6μm thick silicon film deposited on the copper substrate thus obtained maintained constantly around 2000 mAh g^{-1} during 50 cycles [13]. Silicon film electrode is very suitable for micro-batteries, but the use of physical methods such as magnetron sputtering preparation, and the cost is very high, therefore, difficult to mass production.

2 Improving the binders

In commercial lithium-ion batteries, poly(vinylidene fluoride) (PVdF) has been used as binder for both the negative and positive electrodes because of its good electrochemical stability and high adhesion to the electrode materials and current collectors. However, conventional PVDF binder is easy to absorb the electrolyte and swell, resulting in decreased bond ability. On the one hand, to explore new high-performance binder, Buqa et al. [14] showed that 10% nano-Si containing graphite electrodes using 1% SBR/1% CMC binder have a better cycling behavior than ones using 10% PVDF binder. They concluded that the use of SBR and CMC binder

enhanced the adhesion strength, and their contents should be kept at < 6% to avoid hindering the lithium-ion diffusion. On the other hand, it is modified the conventional PVDF binder to enhances the cohesive ability and changes the morphologies of electrode to be compact, which are supposed to suppress the volume changes of silicon and stabilize the electrode structure effectively [15, 16].

3 Improving the electrolyte

The formation of SEI film on the electrode surface is due to organic salt and solvents electrochemical reduction, its morphology and composition depend the electrolyte composition. While this layer imparts kinetic stability to the electrolyte against further reduction in successive cycles and thereby ensures good cyclability of the electrode, it leads to irreversible loss of Li and the capacity of the battery. In Chen's paper [17], the effect of VC as electrolyte additive on the electrochemical performance of Si film anode was studied. The cycle performance and efficiency of Si film anode were enhanced significantly with the presence of VC in electrolyte. It was found that the SEI layer formed in VC-containing electrolyte possessed better properties. It was impermeable to electrolyte and its impedance kept almost invariant upon cycling. The presence of VC in electrolyte brought out the VC-reduced products and decreased the LiF content in SEI layer. The major components of SEI layer were similar in VC-free and VC-containing electrolytes, which contained lithium salt (e.g. $ROCO_2Li$, Li_2CO3, LiF), polycarbonate and silicon oxide. It was newly found that silicon oxide could be formed in SEI layer of Si film anode due to the reaction of lithiated silicon with permeated electrolyte in both VC-free and VC-containing electrolytes.

4 Improving the current collector and electrode structure

To overcome poor cycle-life problem of silicon, several approaches have been

suggested. However, until now the cycling stability has not been satisfactory. This is mainly attributed to a loss of electric contact among particles and delamination of electrode layer from the current collector, which is caused by volume change of Si-based anode materials during cycling. There is a need for an improved lithium-ion battery with Si-based anodes in which the interface between the anode current collector and the Si based active material has a good adhesion. Kim et al. reported [18] that cycle performance of the mixed silicon-graphite composite electrode, with a specific capacity of about 800 mAh g^{-1}, for lithium-ion batteries has significantly been improved by using a Cu current collector with a properly modified surface morphology. Especially, it is found that the electrode slurry-coated on a nodule-type foil exhibits a quite good capacity retention. The enhanced cyclability was attributed to the formation of the micro-columnar structure in the composite electrode layer during cycling, and thereby the electrode layer can strongly stick to the current collector and does not lose the electric contact with the current collector.

Despite improved binder, electrolyte, current collections means can be improved to some extent, but the electrochemical properties of the silicon-based material achieve a breakthrough is still the key to the commercialization. The main strategy to improve the silicon-based material is to design a composition and microstructure of materials to suit the volume effect of silicon and maintain the electrode conductive. The main ways is nano-technology, composite, etc.. Taking into account the large-scale production and manufacturing costs, preparation of composite materials should be the mainstream of the development of silicon-based anode.

5 Si-C composite materials

From an application standpoint, a considerable improvement in the first cycle

efficiency and the cycling life remains to be done for such anode systems. Carbon has been used as an active matrix because of its softness and compliance, relatively low mass, good electronic conductivity, reasonable Li-insertion ability, and small volume expansion. There has been another attention that focuses on composites consisting of silicon and carbon composite. Work on Si-C composite anodes started in the early 1990s. Dahn et al. appear to have been the first to prepare Si/C composites from various polymers containing silicon and carbon. The first anode was prepared from thermal pyrolysis of polymethylphenylsiloxane (PMPS) and polyphenylsesquisiloxane (PPSSO) polymers in the 900-1300 ºC temperature range [19]. When pyrolysis was performed at 1300 ºC and above, anodes showed low reversible capacities (close to 200 mAh g^{-1}) and large irreversible capacities because complete oxygen removal occurred with formation of silicon carbide.

Various methods have been employed for preparing Si-C composite anodes. Based on their microstructure, we classify Si-C composite anodes into five types:

5.1 Core-Shell Type

Yoshio et al. [20] reported a care-shell carbon-coated Si composite prepared by thermal vapor decomposition (TVD) method. Carbon-coating in the outer layer plays a very important role in the improvement of the electrochemical behavior. It could not only considerably suppress the big decomposition of electrolytes on the surface of Si-based electrodes, but also provide integral and continuous electric contact networks.

Ng et al. [21-23] prepared a spheroidal carbon-coated Si nanocomposite. The carbon-coated Si nanocomposites spray-pyrolyzed in air at 400 °C show the best cycling performance, retaining a specific capacity of 1120 mAh g^{-1} beyond 100 cycles. The beneficial effect of the carbon coating is enhancing the dimensional stability of the

Si nanoparticles during the Li-insertion and extraction, which then significantly improved the electrical conductivity of the composites.

Highly lithium-electroactive Si quantum dots (n-Si), coated with an amorphous carbon layer were prepared by of butyl-capped Si annealing at 700 or 900 ◦C [24]. The annealed n-Si, capped with a carbon layer, exhibited significantly improved capacity and capacity retention, as compared to conventional Si nanoparticles. In particular, n-Si, annealed at 900 ◦C, showed uniformly dispersed particles with a carbon layer thickness of 1 nm and did not show any SiOx contamination. These particles showed a first charge capacity of 1257 mAh g^{-1}, with an irreversible capacity loss of 29%. Furthermore, capacity retention after 30 cycles was 84%.

Kim et al. reported a synthetic method using reverse micelles at high pressure and temperature in a bomb that produces Si nanoparticles (n-Si) show 5-20 nm sizes, what is more, carbon-coated 10 nm sized n-Si showed 98% efficiency up to 40 cycles [25].

Hu et al. described [26] a Si@SiOx/C nanocomposites in water by the hydrothermal carbonization of glucose in the presence of Si nanoparticles. When the Si@SiOx/C nanocomposite electrode was cycled in the VC-containing electrolyte, an excellent cycling performance was achieved. The reversible capacity is as high as 1100 $mAhg^{-1}$, with no further decay of capacity even after 60 cycles. However, the Si@SiOx/C nanocomposite electrode in the VC-free electrolyte, show a poor cyclability.

Polymer pyrolysis preparation of amorphous carbon coated silicon is a commonly used method. A nanosized anode material with silicon as core and amorphous carbon as shell was synthesized by dispersing nanosized silicon in polyvinylidene fluoride solution and a subsequent pyrolysis process [27]. The first reversible capacity of 1328.8mAh g^{-1}, furthermore, capacity retention after 30 cycles was 97%.

5.2 Fibrous Type

One-dimensional material (nanowire, nanobelt and nanotube) has not only high strength, toughness, in addition, have a large gap in the fibers boundary, it can buffer external stress and its volume change. Fibrous type Si-C composite can be divided into silica fibre-carbon and carboform-silicon.

Carbon-coated silicon nanowire array films prepared by metal catalytic etching of silicon wafers and pyrolyzing of carbon aerogel were used for anodes [28]. The films exhibited an excellent first reversible capacity of 2810 mAh g^{-1}, but the cycling performance is not satisfactory.

Kim et al. [29] reported a mesoporous silicon-carbon nanowires prepared by a SBA-15 hard template. Fig. 1 shows the schematic view of the preparation of the silicon-carbon nanowires, microstructure and cycling performance. The mesoporous silicon-carbon nanowires shows a excellent rate capabilities, the charge capacities at the 2 C rate were 2462 mA h g^{-1}, in addition, it also shows a excellent cycling performance. It is attributed to the mesoporous materials have ordered internal pores, and it can be ensured an even distribution of electrolyte in contact with the electrode surface. The thin walls, of uniform dimensions throughout, ensure short diffusion paths for lithium ions on Li-insertion/extraction and electrons and hence equal high rates

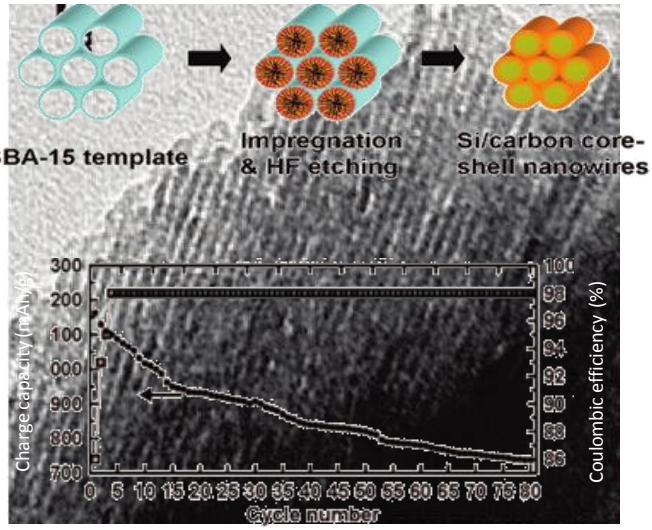

Fig. 1 Schematic view of the preparation of mesoporous silicon-carbon composite nanowires, microstructure and cycling performance [29]

of transport throughout the material.

Si nanotubes were prepared by reductive decomposition of a silicon precursor in the alumina template and etching [30]. These nanotubes showed impressive results, which had very high reversible charge capacity of 3247 mA h g^{-1} with Coulombic efficiency of 89% and also demonstrated superior capacity retention even at a 5C rate. Furthermore, the capacity in Li-ion full cell consisting of cathode $LiCoO_2$ and anode Si nanotube demonstrated 10 times higher capacity than commercially available graphite even after 200 cycles. The high electrochemical performance is believed to be due to the unique open tubular structure of silicon which increases the contact between the silicon and electrolyte, and the thin carbon layer, which minimizes the direct contact between the Si and electrolyte and promotes the formation of a stable SEI layer on the inner and outer surface of the Si nanotubes.

Recently, Ji and Zhang [31] reported a high-performance Si and carbon nanofiber composite with a porous structure. The composite was fabricated simply by electrospinning and subsequent carbonization of the mixture of polyacrylonitrile (PAN), poly-l-lactic acid (PLLA) and nano-Si. The resultant porous nano-Si and carbon nanofiber composite anodes exhibited a high initial reversible capacity of 1100mAh g^{-1}, and a high first cycle coulombic efficiency of 82.1%. However, the reversible capacity retention was not so good. The initial capacity of 1100mAh g^{-1} was decreased to 600mAh g^{-1} after 30 cycles.

Chemical Vapor Deposition (CVD) method is an effective way to prepare carboform-silicon nanocomposites. Shu et al. [32] reported a coiled carbon nanotubes with different length were grown on superfine silicon particles via a chemical vapor deposition method. As anode active materials, this CNTs/Si composite shows a

reversible specific capacity of 940 mAh g^{-1}, a coulombic efficiency of 80% for the first cycle and good cycling performance. The improvement of the cyclic performance for silicon particles is related to the maintaining of the electronic contact during cycling and forming a thick SEI film on it. Furthermore, Liu et al. [33] synthesized a CNF/Si composite which was prepared in situ by growing carbon nanofibers on the surface of silicon particles by CVD method. Electrochemical measurements indicated that the composite showed higher reversible capacity for 1042 mAh g^{-1} and better cyclability. We believe that improved performance should be attributed to the CNF or CNT on the surface of Si particle which can provide highly flexible space to relieve volumetric expansion when charging, and they can also improve the electric conductivity between Si particles.

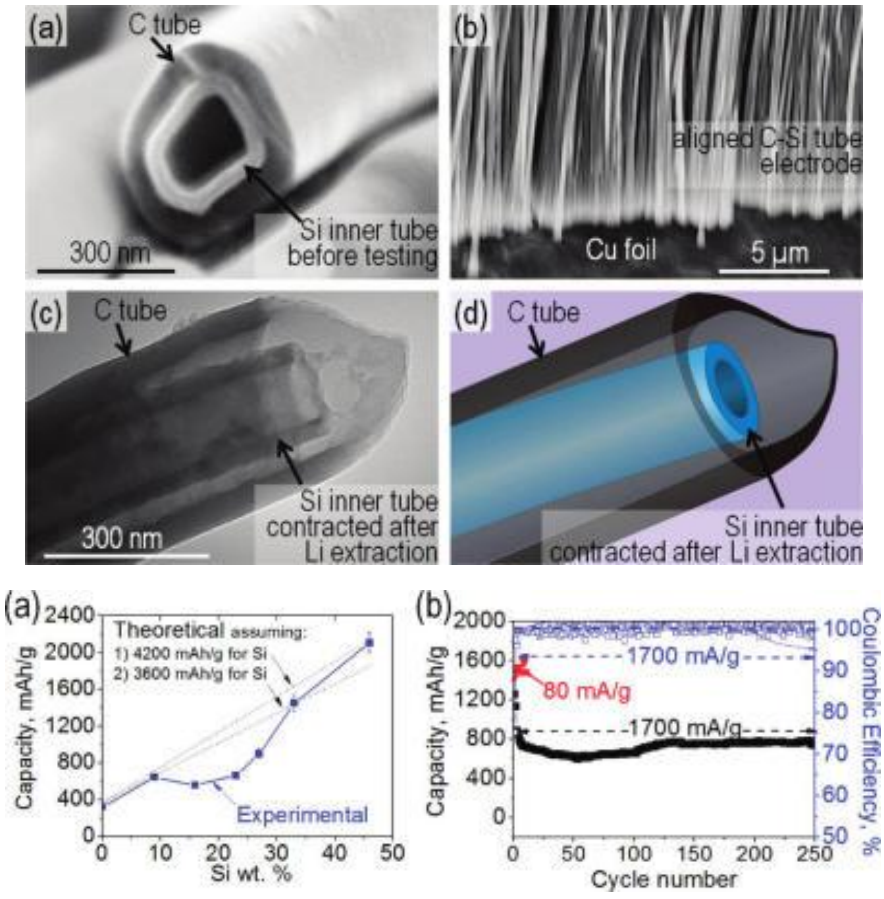

Fig. 2 Microstructures of the composite carbon-silicon tube and its electrochemical property. [34]

Herzbery et al. [34] proposed a simple model to predict shape changes in Si upon electrochemical reaction with Li in a nano-confined geometry. The produced porous Si with a rigid C outer shell showed high capacity, stable performance, and outstanding coulombic efficiency. Microstructures of the composite carbon-silicon tube and its electrochemical property are showed in Fig. 2. The CNT walls were demonstrated to be capable of withstanding stresses caused by the initial Si expansion and Li intercalation. We believe that improved performance should be attributed to its unique structure of nested tubes, the outer tube to ensure a complete carbon interior surface of the silicon tube and the stability of SEI film.

5.3 Multihole Type

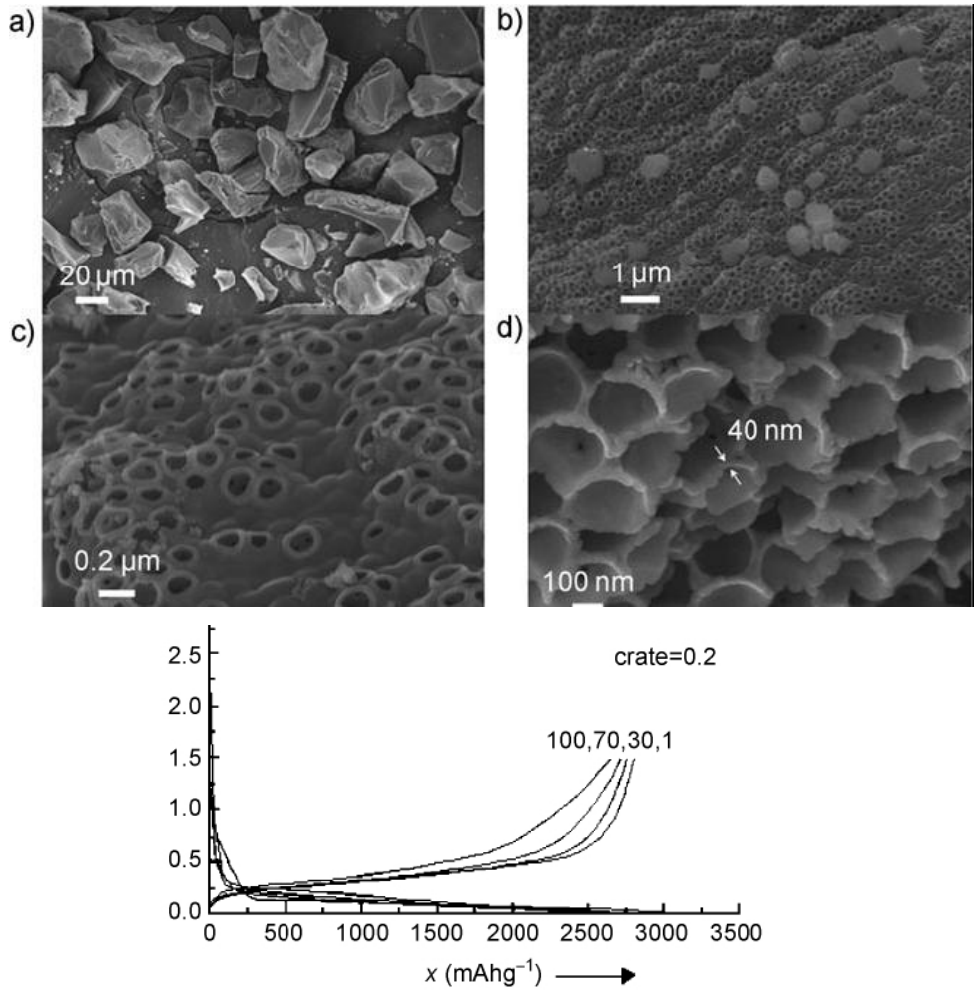

Fig. 3 SEM micrographs of the three dimensional porous silicon carbon nanocomposite and its electrochemical performance [35]

Recently, Kim et al. [35] reported a versatile synthetic method for the formation of three dimensional (3D) porous bulk Si particles by the thermal annealing and etching of physical composites obtained from butyl-capped Si gels and SiO_2 nanoparticles at 900 ºC under an Ar atmosphere. Complete etching of the SiO_2 from the SiO_2/carbon-coated Si (c-Si) composite results in the retention of the remaining c-Si as a highly porous but interconnected structure, thus preserving the starting morphology. A thin pore-wall size of approximately 40 nm can accommodate large strains without pulverization, even after 100 cycles, and a maintained charge capacity of greater than 2800 $mAhg^{-1}$ at a rate of 1 C. SEM micrographs of the 3D porous silicon carbon nanocomposite and its electrochemical performance are showed in Fig. 3.

5.4 Embedded Type

Embedded type Si-C composite materials, active silicon particles embedded in the conductive carbon matrix to buffer the silicon volume effect.

(1) Embedded in amorphous carbon

Formerly, we found [36] a low irreversible capacity in the Si-Ccomposite anode, where carbon was deposited on fine Si particles (<1μm) by thermal decomposition of polyvinylchloride (PVC). The composite anode showed a high first cycle coulombic efficiency of 82% and a high reversible capacity of about $1000mAhg^{-1}$.In addition, the capacity degradation rate during cycling was as high as 0.93% per cycle. In our recent report [37], several sizes of silicon particles were coated with carbon by thermal decomposition of PVC and chlorinated polyethylene (CPE), and the effect of size of silicon particles and the Si-C ratio of the Si-C composite anode on the electrochemical performances was examined. The best result in the study is found in the carbon–50nm Si by pyrolysis of the mixture of 10 wt.% Si-90 wt.% PVC (chlorine content: 56.8

wt.%) at 900 ◦C for 2 h, where the carbon content is 48 wt.%. The first cycle charge-discharge coulombic efficiency is 69.2%, the reversible capacity 970mAh g^{-1}, and the capacity fade upon cycling 0.24% per cycle.

(2) Embedded in graphite

Alkali-metal graphite-intercalation compounds with different carbon-metal atomic ratios, used KC_8 have been oxidized by $SiCl_4$ to synthesize silicon-graphite composites [38]. The result show that nanocrystallized silicon particles well dispersed in the graphite matrix.

(3) Embedded in graphene

Si/graphene composite was prepared by simply mixing of commercially available nanosize Si and graphene. Electrochemical tests show that the Si/graphene composite maintains a capacity of 1168 mAh g^{-1} and an average coulombic efficiency of 93% up to 30 cycles [39]. Wang et al. reported a grapheme-silicon nonocomposite [40]. The graphene-silicon nanocomposite film was prepared by an in-situ chemical method using graphite oxide as the precursor. The graphite oxide was synthesized from natural graphite powder by a modified Hummers method. The electrochemical results show that graphene-Si composite film has much higher discharge capacity beyond 100 cycles (708 mAh g^{-1}) than that of the cell with pure graphene (304 mAh g^{-1}). The graphene functions as a flexible mechanical support for strain release, offering an efficient electrically conducting channel, while the nanosized silicon provides the high capacity.

5.5 Diversified Type

To consider the structure, this is a relatively ideal dispersion system, nano-silicon active molecules highly dispersed in the carbon layer, to the greatest extent possible to overcome the silicon volume expansion.

Wilson et al. reported [41] that blends of pitch and silane polymers, $(Me_2Si)x(PhMeSi)y$, with various pitch/polymer ratios were pyrolysed at 1000 °C. Some of the pyrolysed mixtures demonstrated large reversible capacities for lithium insertion (over 600 mAh g^{-1}), small irreversible capacities (150-200 mAh g^{-1}) and small hysteresis between charge and discharge cycles. Similarity, Wilson et al. [42] also reported nanodispersed silicon in carbon by CVD methods. The silicon is located in the unorganized regions of the carbon and the organized regions are little affected by its presence. The silicon performs as hoped, increasing the capacity of the materials by taking advantage of the high lithium alloying capacity of silicon, while retaining the high reversibility of the carbon.

In this paper, we have investigated the Si-based material-C composite electrode for Li-ion batteries. The report is divided in to two parts:

Part 1 is described the Si-based material-C composite electrode in liquid electrolytes.

Part 2 is described the carbon coated nano-Si composite with CNF electrode which explained the part 1 in PEO (polyethylene oxide) electrolytes.

References:

[1] J.M. Tarascon, M. Armand, Nature, 414 (2001) 359.

[2] A.N. Dey, J. Electrochem. Soc., 118 (1971) 1547.

[3] R.A. Sharma, R.N. Seefurth, J. Electrochem. Soc. 123 (1976) 1763.

[4] B.A. Boukamp, G.C. Lesh, R.A. Huggins, J. Electrochem. Soc. 128 (1981) 725.

[5] H. Li, X. Huang, L. Chen, Z. Wu, Y. Liang. Electrochem. Solid State Lett., 2 (1999) 547.

[6] H. Ma, F. Cheng, J. Chen, J. Zhao, C. Li, Z. Tao, J. Liang. Adv. Mater., 19 (2007)

4067.

[7] H. Li, X. J. Huang, L. Q. Chen, G. W. Zhou, Z. Zhang, D. P. Yu, Y. J. Mo, N. Pei. Solid State Ionics, 135 (1/4) (2000) 181.

[8] L. F. Cui, R. Ruffo, C. K. Chan, H. Peng, Y. Cui. Nano Lett., 9 (2008) 491.

[9] C. K. Chan, R. N. Patel, M. J. O'Connell, B. A. Korgel, Y. Cui. ACS Nano, 4 (3) (2010) 1443.

[10] T. Song, J. Xia, J. H. Lee, D. H. Lee, M. S. Kwon, J. M. Choi, J. Wu, S. K. Doo, H. Chang, W. I. Park, D. S. Zang, H. Kim, Y. Huang, K. C. Hwang, J. A. Rogers, U. Paik. Nano Lett., 10 (5) (2010) 1710.

[11] H. Föll, H. Hartz, E. Ossei-Wusu, J. Carstensen, O. Riemenschneider. Phys. Status Solidi-R., 4 (1/2) (2010) 4.

[12] C. K. Chan, H. Peng, G. Liu, K. McIlwrath, X. F. Zhang, R. A Huggins, Y. Cui. Nat. Nano, 3 (1) (2008) 31.

[13] M. Uehara, J. Suzuki, K. Tamura, K. Sekine, J. Takamura. J. Power Sources, 146(1/2) (2005) 441.

[14] H. Buqa, M. Holzapfel, F. Krumeich, C. Veit, P. Novák. J. Power Sources, 161 (2006) 617.

[15] J. Li, L. Christensen, M. N. Obrovac, K. C. Hewitt, J. R. Dahn. J.Electrochem. Soc., 155 (3) (2008) A234.

[16] Y. Xu, G. Yin, Y. Ma, P. Zuo, X. Cheng. J. Power Sources, 195 (7) (2010) 2069.

[17] L. B. Chen, K. Wang, X. H. Xie, J.Y. Xie. J. Power Sources, 174 (2007) 538.

[18] Y. L. Kim, Y. K. Sun, S. M. Lee. Electrochim. Acta, 53 (13) (2008) 4500.

[19] A.M.Wilson, J.N. Reimers, E.W. Fuller, J.R. Dahn, Solid State Ionics 74 (1994) 249.

[20] M. Yoshio, H. Wang, K. Fukuda, T. Umeno, N. Dimov, Z. Ogumi. J. Electrochem. Soc., 149 (2002) A1598.

[21] S. H. Ng, J. Wang, D. Wexler, K. Konstantinov, Z. P. Guo, H. K. Liu. Angew. Chem. Int. Ed., 45 (41) (2006) 6896.

[22] S. H. Ng, J. Wang, D. Wexler, S. Y. Chew, H. K. Liu. J. Phys. Chem. C, 111 (29) (2007) 11131.

[23] S. H. Ng, J. Wang, K. Konstantinov, D. Wexler, S. Y. Chew, Z. P. Guo, H. K. Liu. J. Power Sources, 174 (2) (2007) 823.

[24] Y. Kwon, G. Park, J. Cho. Electrochim. Acta, 52 (14) (2007) 4663.

[25] H. Kim, M. Seo, M. H. Park, J. Cho. Angew. Chem. Int. Ed., 49 (12) (2010) 2146.

[26] Y. S. Hu, R. Demir-Cakan, M. M. Titirici, J. O. Müller, R. Schlögl, M. Antonietti, J. Maier. Angew. Chem. Int. Ed., 47 (9) (2008) 1645.

[27] Y. Xu, Y. Yin, Y. Ma, P. Zuo, X. Cheng. J. Mater. Chem., 20 (16) (2010) 3216.

[28] R. Huang, X. Fan, W. Shen, J. Zhu. Appl. Phys. Lett., 95 (13) (2009) 133119.

[29] H. Kim, J. Cho. Nano Lett., 8 (11) (2008) 3688.

[30] M. H. Park, M. G. Kim, J. Joo, K. Kim, J. Kim, S. Ahn, Y. Cui, J. Cho. Nano Lett., 9 (11) (2009) 3844.

[31] J. Ji, X. Zhang. Electrochem. Commun., 11 (6) (2009) 1146.

[32] J. Shu, H. Li, R. Z. Yang, Y. Shi, X. J. Huang. Electrochem.Commun., 8 (1) (2006) 51.

[33] H. P. Liu, W. M. Qiao, L. Zhan, L. C. Ling. New Carbon Mater., 24 (2) (2009) 124.

[34] B. Hertzberg, A. Alexeev, G. Yushin. J. Am. Chem. Soc., 132 (25) (2010) 8548.

[35] H. Kim, B. Han, J. Choo, J. Cho. Angew. Chem. Int. Ed., 47 (52) (2008) 10151.

[36] Y. Liu, K. Hanai, J. Yang, N. Imanishi, A. Hirano, Y. Takeda. Electrochem, Solid-

State Lett. 7 (2004) A369.

[37] Q. Si, K. Hanai, N. Imanishi, M. Kubo, A. Hirano, Y. Takeda, O. Yamamoto. J. Po7wer Sources 189 (2009) 761.

[38] S. Cahen, R. Janot, L. Laffont-Dantras, J. M. Tarascon. J. Electrochem. Soc., 155 (7) (2008) A512.

[39] S. L. Chou, K. B. Wang, M. Choucair, H. K. Liu, J. A. Stride, S. X. Dou. Electrochem. Commun., 12 (2) (2010) 303.

[40] J. Wang, C. Zhong, S. Chou, H. Liu. Electrochem. Commun., 12 (11) (2010) 1467.

[41] W. Xing, A. M. Wilson, G. Zank, J. R. Dahn. Solid State Ionics, 93 (3/4) (1997) 239.

[42] A. M. Wilson, J. R. Dahn. J. Electrochem. Soc., 142 (2) (1995) 326.

Part 1: Si-based material/C composite electrode in liquid electrolytes based system

In part 1, we described the Si-based material/C composite electrode in liquid electrolytes. Firstly, we prepared several sizes of silicon particles which were coated with carbon by thermal decomposition of PVC and chlorinated polyethylene (CPE), and investigated the effects of size of silicon particles and the Si-C ratio of the Si-C composite anode on the electrochemical performances. Secondly, for further improvement of the electrochemical performance of the electrode cast on copper foil, we investigated the carbon-coated nano-Si anode with CNF added in order to improve the contact with the copper substrate and between the electrode materials. CNF was incorporated into the composite by two methods; one is the direct mixing of CNF with the nano-Si powder coated with carbon produced by pyrolysis of PVC, and other is the mixing of CNF, nano-Si powder, and PVC with subsequent firing. Finally, we investigated a pulverized inexpensive micron size SiO powder mixed with CNF. The electrode performance of the SiO/CNF composite anode was investigated as a function of the milling time and discussed with respect to the change of the Si valence by the milling time. The high irreversible capacity at the first cycle was compensated by chemically precharging with a lithium thin film attached to the composite electrode.

1.1. Highly reversible carbon-nano-silicon composite anodes for lithium rechargeable batteries

1.2. A high performance Si/C composite anode with carbon nanofiber for Li-ion batteries

1.3. Improvement of cyclic behavior of a ball-milled SiO and carbon nanofiber composite anode for lithium-ion batteries

1.1 Highly reversible carbon-nano-silicon composite anodes for lithium rechargeable batteries

1. Background

Many approaches have been reported to reduce the first cycle irreversible capacity and the capacity loss of silicon [1]. A reduction of the particle and crystalline size into the nanometer scale decreased the first cycle irreversible capacity and the improvement of cycling performance. Li et al. [2] reported that a charge capacity of 2775 mAh g^{-1} and a discharge capacity of 2097 mAh g^{-1} could be obtained for a nano-Si anode during the first cycle, giving 76% coulombic efficiency. Its reversible capacity at the 10th cycle was 1729 mAh g^{-1}.The capacity loss during cycling was as high as 1.75% per cycle. While particle size reduction can mitigate the stress of the volume change to a certain degree, it cannot completely eliminate capacity fade upon cycling. Another approach to obtain a high-performance Si anode is to use a Si-C composite anode. Various methods have been employed for preparing Si-C composite anodes. A high reversible capacity was demonstrated by nano-Si on fine graphite particles (KS-6), where 10 - 20 nm Si particles were deposited on the graphite by thermal vapor deposition of silane [3,4]. This anode showed initial charge and discharge capacities of 1350 and 1000 mAh g^{-1}, respectively, and a reversible capacity over 900 mAh g^{-1} was retained after 100 cycles,. However, this preparation method is a little complicate for the commercial application.

We [5] reported a low irreversible capacity in the Si-C composite anode, where carbon was deposited on fine Si particles (<1μm) by thermal decomposition of polyvinylchloride (PVC). The composite anode showed a high first cycle coulombic efficiency of 82% and a high reversible capacity of about 1000 mAh g^{-1}. However, the

capacity decreasing rate during cycling was as high as 0.93% per cycle. In this study, several sizes of silicon particles were coated with carbon by thermal decomposition of PVC and chlorinated polyethylene (CPE), and the effect of size of silicon particles and the Si/C ratio of the Si-C composite anode on the electrochemical performances was examined. The carbon-nano-Si composite showed a high revertible capacity and an excellent cycling performance.

2. Experimental

The carbon-silicon composites were prepared by the method reported in the previous paper [5]. The silicon powders of 10 μm and 4 μm size were purchased from High Purity Chemicals, Japan, that of 0.7 μm size from Kinsei Matec, Japan, and 50 nm size from Aldrich. CPE with the different content of chlorine was supplied by Kureha Elastmer, Japan, and PVC was supplied by Aldrich. PVC (or CPE) was mixed with the silicon powders in tetrahydrofuran (THF), and dried at 60 ºC for 5 h, then the mixed powders were heated at 900 ºC for 2 h in 2% H_2-Ar. Elemental analysis of Si and C contents in the Si-C composite was performed using a Yanaco MT-2 CHN corder.

The electrochemical tests of the carbon-Si composite electrodes were carried out with a two-electrode coin-type cell. The working electrode was composed of 60 wt.% carbon-Si, 20 wt.% acetylene black (AB), and 20 wt.% poly (vinylidene fluoride) (PVDF). The carbon-Si composite and AB were mixed in a 0.02 g ml^{-1} PVDF/1-methl-2-pyrrolidone solution, and the viscous mixture was casted on a 300 μm thick nickel foam, which was served as a current collector. The electrode was further dried at 120 ºC under vacuum for 1 h followed by pressing at 400 kgf cm^{-2}. The geometric area of the electrodes was about 0.8 cm^2 and the typical thickness was about

220 μm. The 2025 coin-type cells were assembled in an Ar-filled glove box using 1M $LiClO_4$ in ethylene carbonate (EC) and diethylene carbonate (DEC) (1:1 in volume) as the electrolyte and metallic lithium foil (20 μm in thickness) as the counter electrode. The electrochemical performance of the composite anode was evaluated using constant current (0.1 C rate) charge-discharge cycling in the voltage range 20-1500 mV at room temperature. The electrode capacity was calculated from the weight of active material, e.g. Si-C weight.

X-ray diffraction (XRD) patterns were obtained using Rigaku Rotaflex RU-200B with Cu-Kα radiation. The morphology of the composite electrode was examined with a help of scanning electron microscopy (SEM) (Hitachi SEM S-4000) and transmission electron microscopy (TEM) (Hitachi TEM H900). Raman spectroscopy was used to characterize the deposited carbon using a RNANOR T64000MI with 488 nm laser. Thermal properties of PVC and CPE were measured using a Rigaku Thermo Plus TG8120.

3. Results and discussion

The carbon-Si composites were prepared by pyrolyzing the mixtures of the different sized Si powder and PVC (or CPE) with the different Si : PVC (or CPE) ratios. Fig. 1 shows the typical XRD patterns of the carbon-Si composite, where the different sized Si powder and PVC mixtures (10 : 90 in weight) were heated at 900 ºC for 2 h. The carbon content in the carbon-Si composite was slightly different with the different particle Si sizes and is around 50 wt.%. The XRD patterns show sharp Si peaks while the carbon peak is broad, which suggests that the carbon of the composite is amorphous.

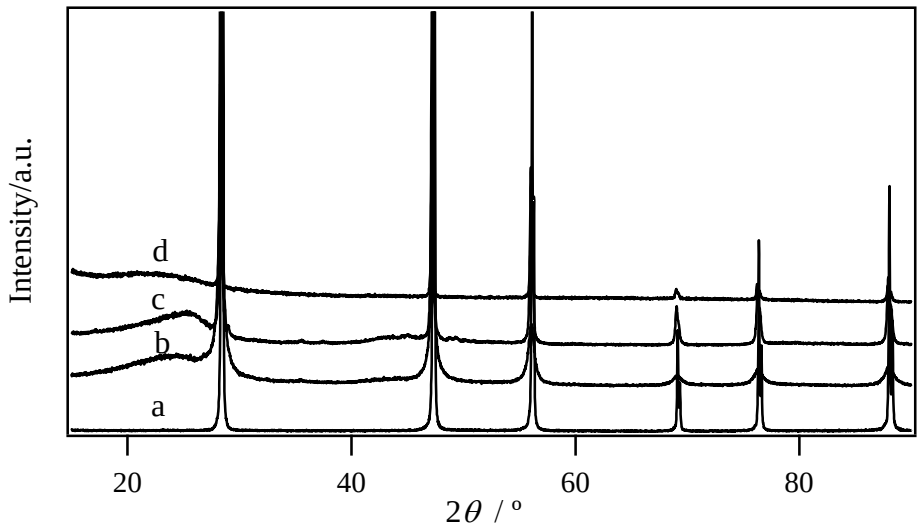

Fig. 1 XRD patterns of carbon-Si composite prepared by pyrolysis of (a) pure Si (4 μm), (b) Si (50 nm)-PVC (10:90 in weight), (c) Si (0.7 μm)-PVC (10:90 in weight), and (d) Si (4 μm)-PVC (10:90 in weight).

Fig. 2 shows Raman spectra of the carbon-Si composite, where carbon was coated on nano-Si powder (50 nm) by pyrolyzing PVC and CPE with the different chlorine contents with a 10 to 90 weight ratio of Si/polymer.

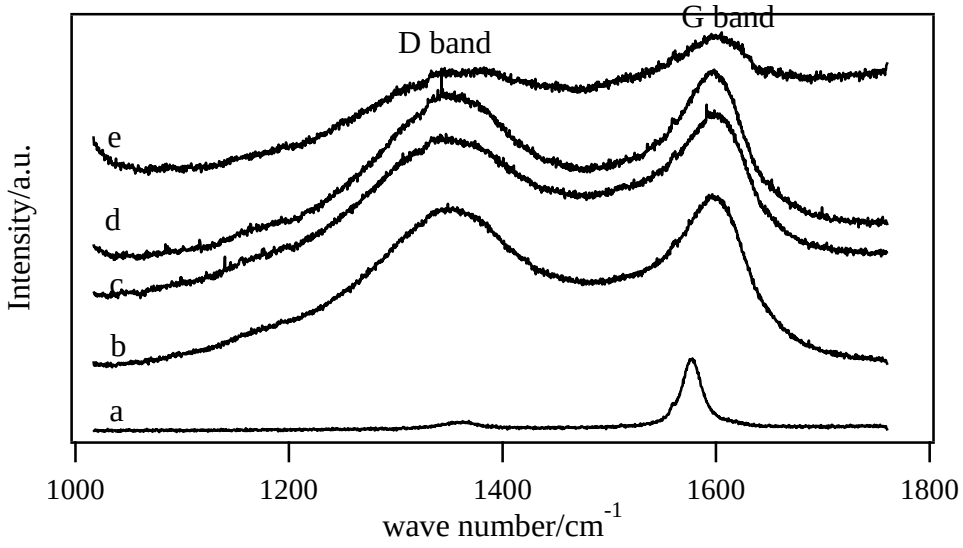

Fig. 2 Raman spectra of (a) MCMB, and carbon-Si composite prepared by pyrolysis of (b) Si (50 nm)-PVC (10:90 in weight), (c) Si (50 nm)-CPE (chlorine 70%) (10: 90 in weight), and (d) Si (50 nm)-CPE (chlorine 39.5%) (10:90 in weight), and (e) Si (50 nm)-CPE (chlorine 25.5%) (10:90 in weight).

Two main peaks are observed at around 1350 and 1580 cm^{-1}, which are designated as the D band and the G band, respectively [6]. The G band is associated with crystalline graphite, while the D band is attributed to amorphous graphitic materials. The relative intensity ratio of the D and G bands, I_G/I_D, gives information about the perfection of the graphite layered structure [7]. The I_G/I_D ratios are listed in Table 1. The effect of the chlorine content in CPE on the I_G/I_D is not clear, but the I_G/I_D ratio of meso-carbon micro beads (MCMB) is almost 11 times higher than that of pyrolyzed carbon, suggesting the pyrolyzed carbon is highly disordered.

Table 1 The relative intensity ratio of the D and G bands (IG/ID) of the carbon-coated Si prepared by pyrolysis of CPE (or PVC)and Si (10: 90 in weight).

Samples	Carbon content wt.%	I_G/I_D
CPE (chlorine 25.5wt.%)	3	1.00
CPE (chlorine 39.5wt.%)	13	0.83
PVC (chlorine 56.8wt.%)	48	0.85
CPE (chlorine 70.0wt.%)	62	0.82
Graphite (MCMB)	100	11.00

SEM and TEM images of the carbon-Si composite show the homogenous carbon distribution over the Si matrix and no deposition on the special spaces of Si matrix as shown in Fig. 3. The anode performance of the carbon-Si composite by pyrolyzing PVC and CPE has been examined and its dependence on the Si size and the pyrolyzing conditions has been investigated. The charge and discharge curves of the carbon-50 nm Si and carbon-4 μm Si are shown in Fig. 4, where the Si and PVC mixture (10:90 weight ratio) was pyrolyzed at 900 ºC for 2 h.

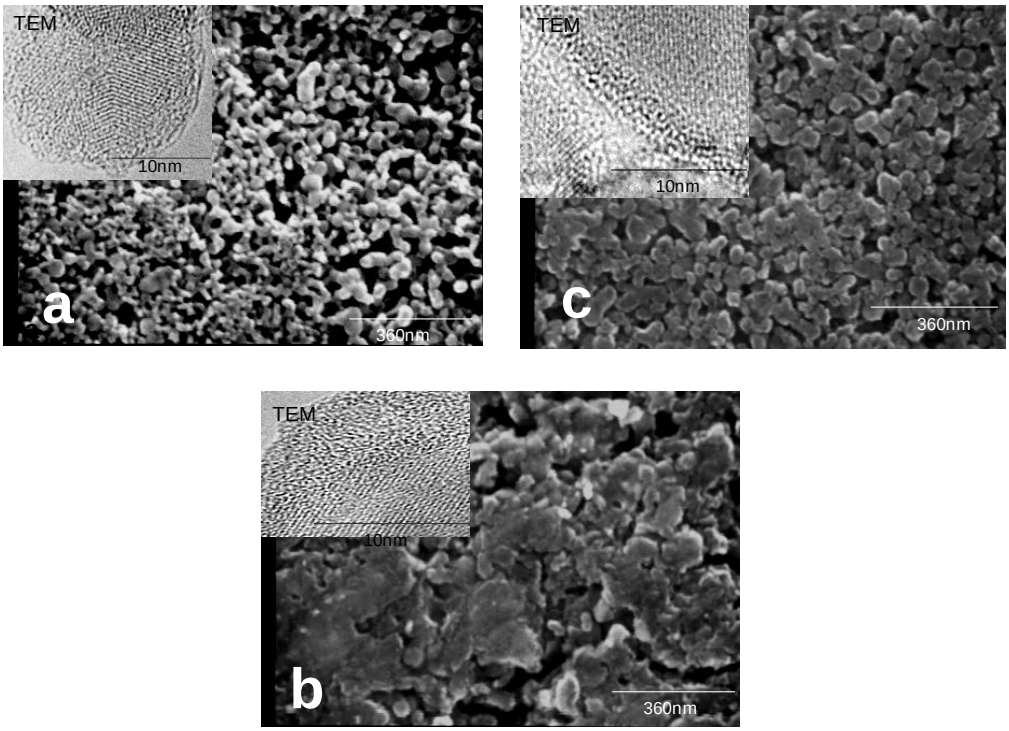

Fig. 3 TEM and SEM images of (a) nano-Si (50 nm), and carbon-Si composite prepared by pyrolysis of (b) Si (50 nm)-PVC (10:90 in weight) and (c) Si (50 nm)-PVC (50:50 in weight).

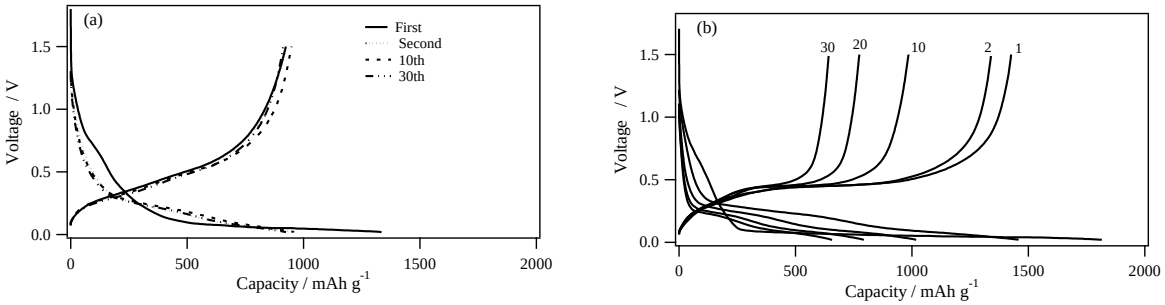

Fig. 4 The charge-discharge curves of carbon-Si composite prepared by pyrolysis of (a) Si (50 nm)-PVC (10:90 in weight) and (b) Si (4 μm)-PVC (10:90 in weight).

In the first discharge capacity (intercalation of lithium into the Si-C electrode) are 1335 mAh g^{-1} for the 50 nm Si-C electrode and 1815 mAh g^{-1} for the 4 μm Si-C electrode, while the charge capacities (deintercalation of lithium from the Si-C

electrode) are 923 mAh g^{-1} for the 50 nm Si-C electrode and 1426 mAh g^{-1} for the 4 μm Si-C electrode. The coulombic efficiency in the first cycle for the 50 nm Si-C electrode is 69.2%, while it is much higher for the 4 μm Si-C electrode (78.6%). The irreversible capacity can be attributed in part to the formation of solid electrolyte interphase (SEI) on the Si and carbon surfaces [8]. This passivation layer is expected to form through a reaction of the lithium with the solvent (EC and DEC) and the salt ($LiClO_4$) of the electrolyte. The amount of the SEI depends on the surface area. It is likely that the large surface area of nano-Si is partially responsible for the higher first cycle irreversible capacity. However, the reversible capacity of carbon-coated Si (large size) decreases rapidly with cycling.

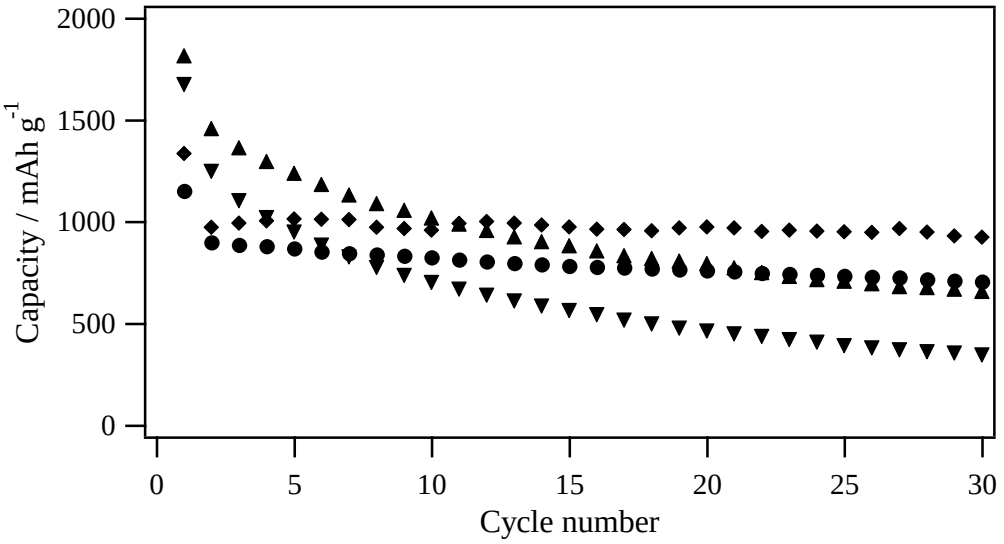

Fig. 5 Cycling performance of carbon-Si composite prepared by pyrolysis of Si-PVC (10:90 in weight) as a function of Si particle size. Cut-off voltage : 20-1500 mV.
◆50nm, ● 0.7 μ m, ▲ 4 μ m, ▼ 10 μ m.

Fig. 5 shows the dependence of the Si size in the carbon-Si composite electrode on

the charge-discharge cycling at room temperature, where Si and PVC weight ratio was 10:90. The content of carbon in the Si-C composite slightly depends on the Si particle size from 58 wt.% to 48 wt.%, which is listed in Table 2.

Table 2 Electrochemical performance of the carbon-coated Si prepared by pyrolysis of PVC and CPE

Starting materials			Si/polymer weight ratio	Carbon content in Si-C (wt.%)	coulombic efficiency in the first cycle (%)	Second cycle discharge capacity (mAh g^{-1})	Capacity fade on cycling (% per cycle) (cycle number)
Polymer	chlorine content in polymer (wt.%)	Si particle size					
CPE	25.5	50 nm	10/90	3	69.3	1968	1.12 (2-30)
CPE	39.5	50 nm	5/95	28	66.5	1441	0.54 (2-40)
CPE	39.5	50 nm	10/90	13	68.3	1740	0.92(2-30)
CPE	39.5	50 nm	20/80	5	67.4	1146	0.90 (2-30)
PVC	56.8	50 nm	10/90	48	69.2	973	0.25 (2-40)
PVC	56.8	50 nm	20/80	31	56.3	951	0.6 (2-30)
PVC	56.8	50 nm	30/70	20	59	1072	0.10 (2-30)
PVC	56.8	50 nm	50/50	7	59	1193	0.83 (2-30)
PVC	56.8	0.7 μm	10/90	58	72.6	898	0.72 (2-30)
PVC	56.8	4 μm	10/90	51	78.6	1457	1.8 (2-30)
PVC	56.8	10 μm	10/90	51	73.5	1248	2.4 (2-30)
CPE	70.0	50 nm	10/90	62	27	324	0.63 (2-30)
CPE	70.0	50 nm	20/80	53	49.4	671	0.2 (2-30)
CPE	70.0	50 nm	30/70	30	56.4	1011	0.16(2-50)

The initial discharge capacities of the Si-C composites with large particle size Si are high. However, the discharge capacity fade upon cycling is very fast for the large size Si. The discharge capacity of the carbon-4 μm Si composite decreases from 1815 mAh g^{-1} in the first cycle to 657mAh g^{-1} after 30 cycles. On the other hand, the carbon-50 nm Si shows a stable cycling performance. A discharge capacity of 1335 mAh g^{-1} in the first

cycle decreases to 880 mAh g^{-1} in the 40th cycle. The carbon-large size Si as 10 μm composite shows a high first discharge capacity of 1674 mAh g^{-1} and the capacity decreases quickly to 344 mAh g^{-1} in the 30th cycle. The carbon-nano-Si composite by pyrolyzing PVC shows a high reversible capacity of about 900 mAh g^{-1}, a high coulombic efficiency of 69.2% in the first cycle, and a low capacity degradation rate of 0.24% per cycle. These electrochemical performances of the electrode are compared with those of the carbon-free nano-Si (mean diameter: 12 nm) reported by Graetz et al. [8], where the first cycle discharge capacity and the coulombic efficiency were 1000 mAh g-1 and 41%, respectively, and the capacity degradation rate was 1.0% per cycle. Li et al. [2] also reported the electrochemical performance of nano-size Si (mean size: 78 nm). The first cycle discharge capacity was as high as 2000 mAh g^{-1}, but the capacity degradation rate was as high as 1.8% per cycle. It means that the carbon-nano-Si composite is quite effective to improve the cycling performance as well as the charge-discharge coulombic efficiency in the first cycle.

The effect carbon content in the carbon-Si composite on the electrochemical performance has been examined for the nano-Si powders. The nano-Si (50 nm) and PVC mixtures with different ratios were heated in 2% H_2-Ar at 900 ºC for 2 h. The carbon content in the composite electrode decreases with decreasing PVC content in the precursors (see Table 2); a carbon content of 48 wt.% decreases to 20 wt.% by decreasing the PVC content from 90 wt.% to 70 wt.% in the Si-PVC precursors.

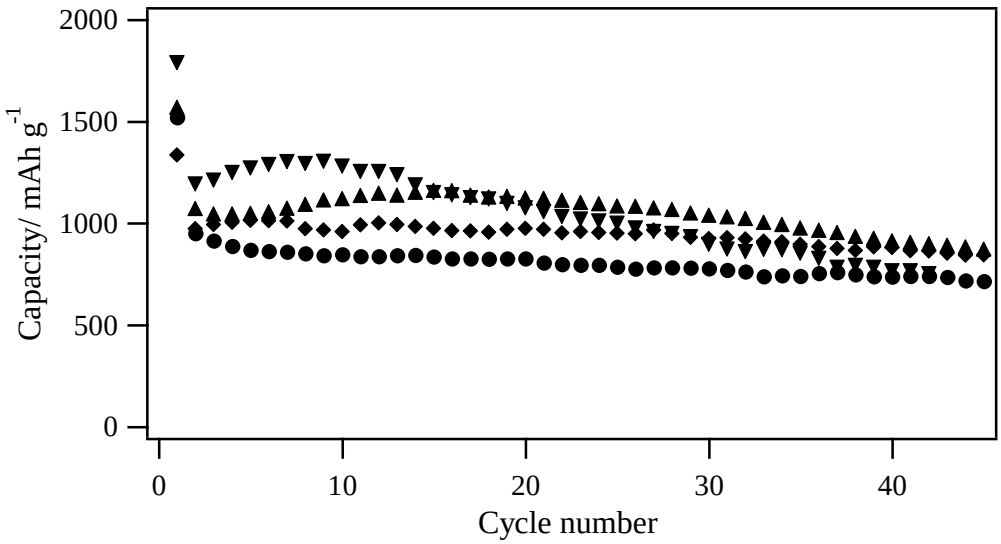

Fig. 6 Cycling performance of carbon-Si composite prepared by pyrolysis of Si (50 nm)-PVC with different compositions. Cut-off voltage : 20-1500 mV.

◆Si-PVC 10:90 in weight (Carbon : 48 wt.%), ●Si-PVC 20:80 in weight (Carbon : 31 wt.%), ▲Si-PVC 30:70 in weight (Carbon : 20 wt.%), ▼Si-PVC 50:50 in weight ratio (Carbon : 7 wt.%).

Fig. 6 shows the cycling performance of the carbon-nano-Si composite anode as a function of the carbon content in the composite at room temperature. The carbon-Si composite electrode with a low carbon content of 7 wt.% shows a high discharge capacity of 1800 mAh g^{-1} and a low coulombic efficiency of 58.8% in the first cycle. The capacity fade upon cycling is larger than those with high carbon content. The high carbon content composite gives a high coulombic efficiency in the first cycle and a good cycling performance. The reversible capacity is slightly lower than that of the sample with low carbon content.

Guo et al. [9, 10] reported the electrochemical performance of the Si-C composite anode, where carbon was coated on nano Si (average particle size: 80 nm) by pyrolysis of polyvinyl alcohol (PVA). The initial reversible capacities were found to be 1100 mAh g^{-1} for the composite with 29.6 wt.% carbon and 950 mAh g^{-1} for that with 19.5 wt.%

carbon. The degradation rate of 0.9% per cycle upon cycling was higher than that of our result of 0.24% per cycle. The polymer of PVA used by Guo contained no chlorine. In this study, we have examined the effect of chlorine in the precursor. It is known that PVC eliminated HCl from 200 to 350 ºC, PVC pitch formed at 400-450 ºC, and the pitch is carbonized from 350 to 550 ºC. Adhesive carbonaceous layer was prepared on metal oxides by pyrolysis of PVC [11]. This process depends on the starting polymer materials. We have examined the effect of the chlorine content in the precursor. PVC (chlorine 56.8 wt.%) and CPE with different chlorine contents (70, 39.5 and 25.5 wt.%) were used for the carbonized materials on nano Si (50 nm).

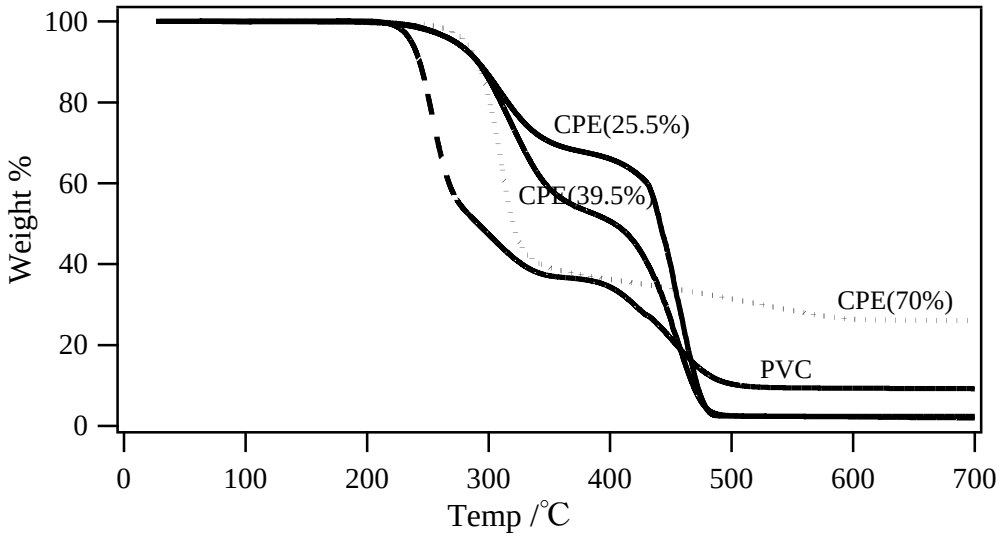

Fig. 7 Thermogravimetric analysis of PVC and CPE.

Fig. 7 shows thermal gravimetric results of PVC and CPE with different chlorine contents. PVC shows two-step decompositions; the first one is between 200 and 350 ºC, and second one between 400 and 500 ºC. The carbonized temperature and the residual carbon content depend on the chlorine content in the polymers. CPE with high chlorine

content shows a high carbonizing temperature and a high residual carbon. The carbonizing temperature may affect the character of the decomposed carbon. However, Raman results show no clear difference for the carbon prepared from the different content of chlorine in the polymers.

Fig. 8 shows the cycling performance of the carbon-nano-Si composite prepared from the polymers with different chlorine contents, along with pure Si (50 nm) and the carbon prepared by pyrolysis of PVC at 900 ºC.

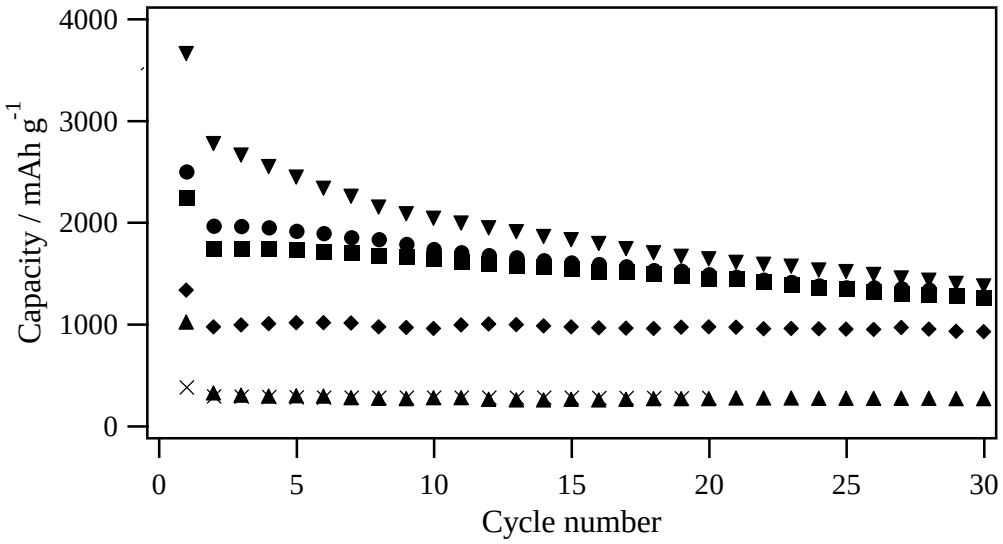

Fig. 8 Cycling performance of carbon-Si composite prepared by pyrolysis of Si-PVC and Si-CPE (10: 90 in weight). Cut-off voltage: 20-1500 mV.

▲ CPE (chlorine: 70%), Carbon 62wt.%, ◆ PVC (chlorine: 56.8%), Carbon 48 wt.%

■ CPE (chlorine: 39.5%), Carbon 13wt.% ● CPE (chlorine: 25.5%), Carbon 3 wt.%

▼ Pure Si × Pure carbon (Pyrolysis of PVC)

The carbon anode without Si shows the coulombic efficiency in the first cycle was 73.8 % and the reversible capacity after second cycles was about 280 mAh g^{-1}. The nano-Si-C composite prepared from CPE with low chlorine content shows a high reversible capacity and a high coulombic efficiency in the first cycle, but the capacity

fade upon cycling is slightly higher than those for the Si-C composites prepared from CPE and PVC with high chlorine content. The Si-C composites prepared from CPE with a low chlorine content show low carbon content (see Table 2). The carbon-nano-Si composite prepared by pyrolysis of Si-CPE (CPE: with 39.5 wt. % chlorine; Si : CPE = 5 : 95 in weight) shows a carbon content of 28 wt. % and a low capacity fade of 0.27% per cycle between 2 and 20 cycles. However, the capacity fade increases upon further cycling. The carbon-nano-Si composite prepared by pyrolysis of CPE with 70 wt. % chlorine give a low coulombic efficiency at the first cycle and low reversible capacity of 324 mAh g^{-1}, where the carbon content in the composite was about 62 wt. %. The composite with 53 wt. % carbon prepared by pyrolysis of CPE with 70 wt. % chlorine also low reversible capacity of 671 mAh g^{-1}. These results suggest that CPE with high content and low chlorine content as the carbon source for the C-Si composite electrode is not suitable to obtain a high-performance anode and PVC is the best candidate for the electrode.

The electrode performances of the carbon-Si composite are summarized in Table 2. The anode performance of the carbon-Si electrode depends strongly on the size of Si particles as well as the carbon content in C-Si composite. The large size Si shows a high initial charge-discharge capacity, but the degradation rate is high. The carbon content in the composite plays an important role. The optimum content is observed. The low carbon content sample shows a low first cycle coulombic efficiency as well as a high carbon content one. The low carbon content sample shows a high reversible capacity, but the capacity fade upon cycling is faster than that of sample with optimized carbon content. The optimum carbon content in nano-size Si is about 50 wt.%.

4. Conclusion

The charge and discharge performances of the carbon-Si composite prepared by pryolysis of PVC and CPE were examined as a function of the particle size of Si powder, carbon content on Si, and the chlorine content in the precursor. The carbon-nano-sized Si composite shows a high coulombic efficiency in the first cycle. A low carbon content nano-Si composite gives a high reversible capacity, but the capacity fade upon cycling is higher than that of high carbon content. The best result in this study is found in the carbon-50 nm Si by pyrolysis of the mixture of 10 wt.% Si-90 wt.% PVC (chlorine content: 56.8 wt.%) at 900 ºC for 2 h, where the carbon content is 48 wt.%. The first cycle charge-discharge coulombic efficiency is 69.2%, the reversible capacity 970 mAh g^{-1}, and the capacity fade upon cycling 0.24% per cycle.

References

[1] U. Kasavajjula, C. Wang, A. L. Appleby, J. Power Sources 163 (2007) 1003.

[2] H. Li, X. Huang, L. Chen, Z. Wu, Y. Liang, Electrochem. Solid-State Lett. 2 (1999) 547.

[3] M. Holzapfel, H. Buqa, F. Frumeich, P. Novak, P. M. Petra, C. Veit, Electrochem. Solid-State Lett. 8 (2005) A516

[4] M. Holzapfe, H. Buqa, W. Scheifele, P. Novak, P. M. Petra, Chem. Commun. 12 (2005) 1566.

[5] Y. Liu, K. Hanai, J. Yang, N. Imanishi, A. Hirano, Y. Takeda, Electrochem. Solid-State Lett. 7 (2004) A369.

[6] M.Yoshikawa, G. Katagiri, H. Ishida, A. Ishitani, Solid State Commun. 66 (1988) 1177.

[7] J. Kastner, T. Pichler, H. Kuzmany, Chem. Phys. Lett. 221 (1994) 53.

[8] J. Grattz, C. C. Ahn, R. Yazami, B. Fultz, Electrochem. Solid-State Lett. 6 (2003) A194.

[9] Z. P. Gao, R. Milin, J. Z. Wang, J. Chen, H. K. Liu, J. Electrochem. Soc. 152 (2005) A2211.

[10] Z. P. Gao, D. Z. Jia, L.Yuan, H. K. Liu, J. Power Sources 159 (2006) 332.

[11] M. Inagaki, Y. Okada, H. Miura, H. Konno, Carbon 37 (1999) 329.

1.2 A high performance Si/C composite anode with carbon nanofiber for Li-ion batteries

1. Background

In the last chapter reported the excellent electrochemical performance of amorphous carbon-coated Si by the pyrolysis of polyvinyl chloride at 900 ºC for 2 h [1]. A composite with 52 wt% nano-Si (particle size of 50 nm) and 48 wt% C had an initial discharge capacity of 970 mA h g^{-1} and a low capacity loss by cycling. However, such high performance was obtained only by the electrode cast onto nickel foam.

Recently, Ji et al. [2] reported a high-performance Si and carbon nanofiber composite with a porous structure. The composite was fabricated simply by electrospinning and subsequent carbonization of the mixture of polyacrylonitrile (PAN), poly-L-lactic acid (PLLA) and nano-Si. The resultant porous nano-Si and carbon nanofiber composite anodes exhibited a high initial reversible capacity of 1100 mA h g^{-1}, and a high first cycle coulombic efficiency of 82.1 %. However, the reversible capacity retention was not so good. The initial capacity of 1100 mA h g^{-1} was decreased to 600 mA h g^{-1} after 30 cycles. Carbon nanofiber (CNF) was suggested as the negative electrode material [3, 4]. CNF features both disordered and graphitic carbon, and this characteristic is expected to overcome the hurdles of lithium batteries for high-power applications, because the CNF anode can deliver high specific capacity even at very high charge-discharge currents, such as a 10 C rate [4-6]. However, the reversible capacity of CNF is not so high and the cyclic performance was poor.

In this study, we have investigated the high performance carbon-coated nano-Si anode further in order to improve the electrochemical performance of the electrode cast on copper foil, with CNF added to the carbon coated nano-Si composite for improved

contact with the copper substrate and between the electrode materials.

2. Experimental

Nano-Si powder (particle size 50 nm, purity >98%) and PVC were purchased from Aldrich and the CNF (diameter: 10-20 nm, length: 0.1-10 μm) was purchased from Jemco, Japan. The nano-Si and carbon composite (Si/C) was prepared as follows; PVC and nano-Si powder (weigh ratio 9:1) were mixed in tetrahydrofuran (THF) and dried at 60 ºC for 5 h. The mixture was then heated at 900 ºC for 2 h in 2% H_2-Ar. The product was mixed with CNF (Si/C:CNF weight ratio 60:10) in 1-methyl-2-pyrrolidone (NMP) solution under ultrasonication for 30 min. and then stirred for 2 h. The carbon coated nano-Si and CNF mixed composite is denoted Si/C/CNF-1. A nano-Si, carbon, and CNF composite was also prepared by another route. Nano-Si, CNF and PVC (weight ratio 1:1:9) were mixed in THF under ultrasonication for 30 min, dried at 60 ºC for 5 h, and then heated at 900 ºC for 2 h in 2%H_2-Ar. The sample obtained by this method is denoted Si/C/CNF-2. A mixed electrode of Si/C/CNF-2 and CNF (weight ratio 75:5) was prepared by the same method as that for Si/C/CNF-1, and was denoted Si/C/CNF-3. On the basis of remaining carbon obtained from heat decomposition of PVC at 900ºC, the Si contents of Si/C, Si/C/CNF-1, Si/C/CNF-2 and Si/C/CNF-3 composites are estimated as about 50%, 43%, 33% and 31%, respectively.

Electrochemical tests of the composite electrodes were conducted using a two-electrode coin-type cell. The working electrodes consisted of the active materials, acetylene black, and poly (vinylidene fluoride) (PVDF) in NMP. The compositions of the electrodes are listed in Table 1.

Table 1. Compositions of composite electrodes (in weight percent).

Electrode	Si/C	Si/C/CNF	CNF	AB	PVDF
Si/C	60%	-	-	20%	20%
Si/C/CNF-1	60%	-	10%	10%	20%
Si/C/CNF-2	-	60%	-	20%	20%
Si/C/CNF-3	-	75%	5%	-	20%

The mixtures of the electrode components in NMP were cast onto copper foils, and dried at 80 ºC for 1 h. The cast electrodes were cut to a size of $1\times1cm^2$. The weights of active material in the electrodes were in the range of 0.2-1 mg. The electrode was further dried at 120 ºC under vacuum for 1 h, followed by pressing at 200 kg f cm^{-2}. Coin-cells (type 2025) were assembled in an Ar-filled glove box using 1 M $LiClO_4$ in an ethylene carbonate (EC) and diethylene carbonate (DEC) mixed solution (1:1 in volume) as the electrolyte and metallic lithium foil (20 μm in thickness) as the counter electrode. The electrochemical performance of the composite anode was evaluated using constant current charge-discharge cycling in the voltage range of 20-1500 mV at room temperature. The specific capacity was based on the weight of Si/C for the Si/C and Si/C/CNF-1 electrodes and that of Si/C/CNF for the Si/C/CNF-2 and Si/C/CNF-3 electrodes.

X-ray diffraction (XRD) patterns were obtained using a Rigaku Rotaflex RU-200B diffractometer with Cu-Kα radiation. The morphology of the composite electrode was examined using scanning electron microscopy (SEM; Hitachi SEM S-4000) and transmission electron microscopy (TEM; JEOL JEM-1011). The impedance measurement was performed using an impedance/gain-phase analyzer (Solartron SI1260) and an electrochemical interface (Solartron SI1287), using a beaker cell with a lithium metal reference electrode. Surface area and porosity measurements were carried

out using a gas absorption analyzer (Shimadzu Micromeritics TriStar 3000).

Table 2. BET surface areas of the Si/C, Si/C/CNF-1, and Si/C/CNF-2 electrode materials.

Material	Total surface area (m^2 g^{-1})	Micropore surface area (m^2 g^{-1})	External Surface area (m^2 g^{-1})
Si/C	29.47	13.59	15.88
Si/C/CNF-1	37.32	0.74	36.59
Si/C/CNF-2	107.05	73.86	33.19

3. Results and discussion

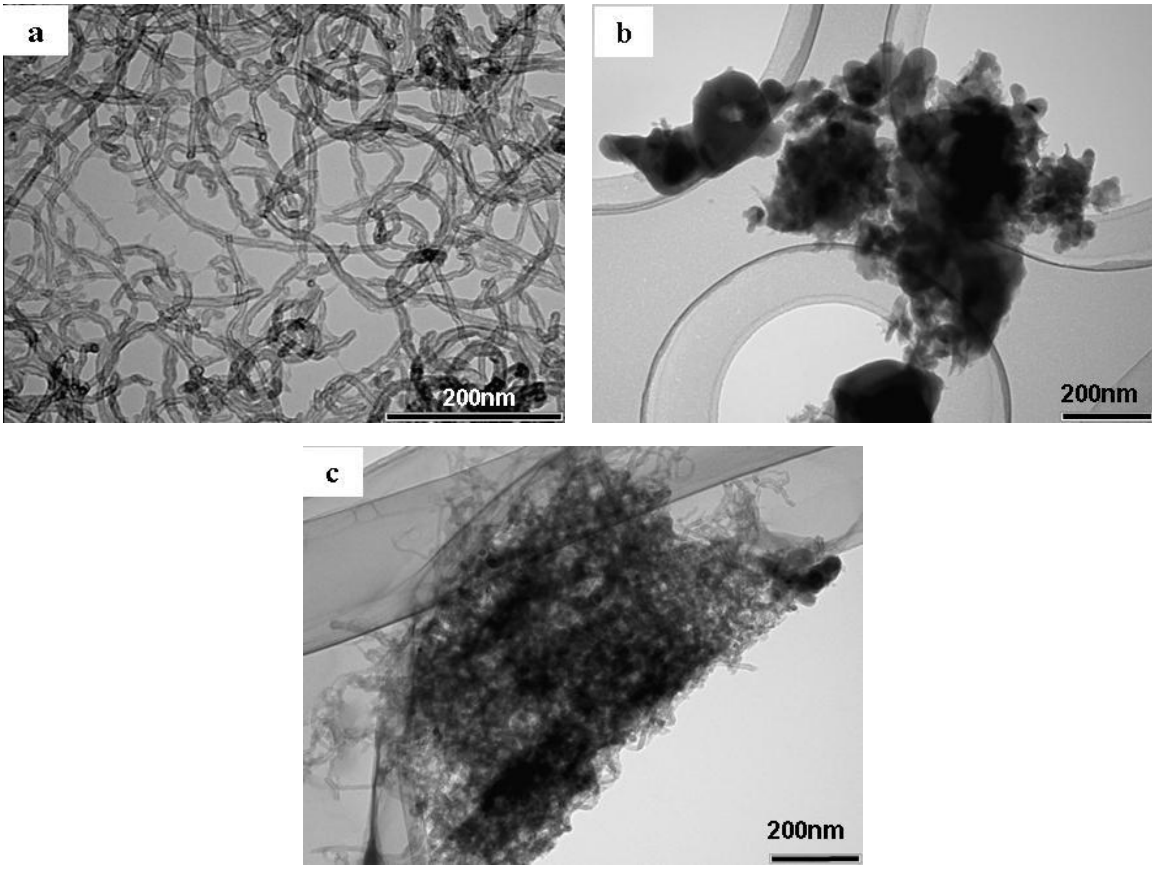

Fig. 1. TEM images of (a) CNF, (b) Si/C, and (c) Si/C/CNF-1.

The surface areas of the composite electrodes measured using the Brunauer-Emmett-Teller (BET) method are shown in Table 2. The surface area of Si/C/CNF-1 is slightly larger than that of Si/C. However, the micropore surface area is

drastically reduced by mixing CNF in Si/C. The micropores in Si/C were diminished during the mixing process, but the mechanism for this is not clear. Fig. 1 shows TEM images of CNF, Si/C, and Si/C/CNF-1. The as-received CNF has a uniform size distribution with a diameter of approximately 20 nm, as shown in Fig. 1a. After ultrasonic mixing with CNF in NMP (see Fig. 1c), the Si/C is uniformly dispersed into the CNF matrix.

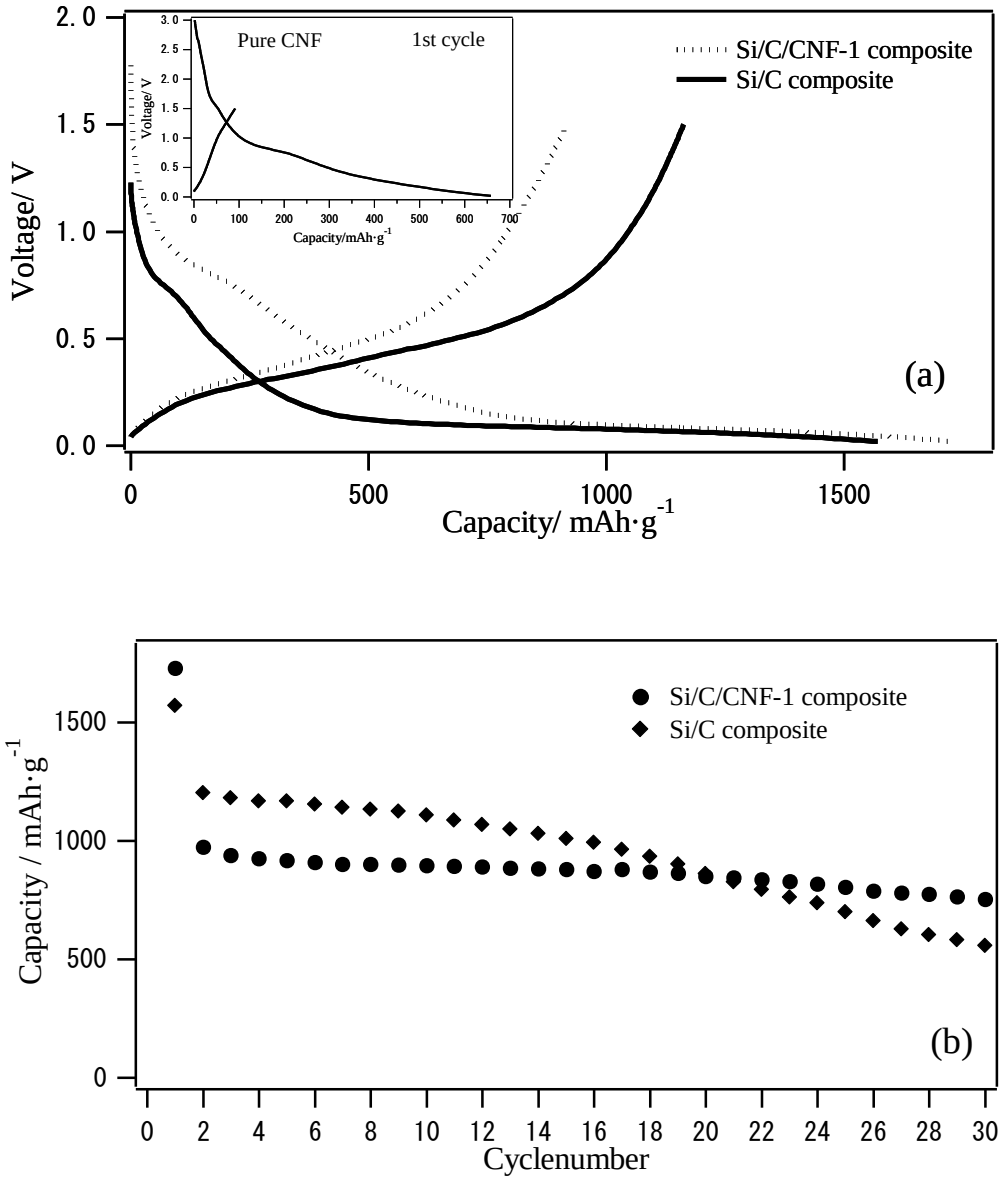

Fig. 2. (a) Voltage vs. lithium insertion capacity curves and (b) cycling performance for Si/C and Si/C/CNF-1 at room temperature. Current rate 1/10 C; Cut-off voltage 20-1500 mV.

Fig. 2 compares the voltage profiles and cycling stability of the Si/C and Si/C/CNF-1 electrodes for lithium insertion and extraction at room temperature. Both electrodes exhibited a sloping potential plateau between 1.1 and 0.1 V in the first lithium insertion process. Si/C/CNF-1 electrode suffered a larger irreversible capacity. The reason can be attributed to the formation of a solid electrolyte interface (SEI) layer, and the trapping of Li ions in the "cuplike" cavity of the bamboo shaped CNF [4]. Li insertion into silicon occurs at potentials below 0.1 V, yielding an extremely large capacity. The coulombic efficiency of Si/C/CNF-1 for the first cycle is 53%, which is lower than that of the bare Si/C composite (74%). This is due to the extremely large irreversible capacity that CNF itself exhibits during the first lithium insertion process, as shown in the inset in Fig. 2a. After the second cycle, the lithium insertion and extraction efficiency was almost 100%. Fig. 2b shows the cycling stability of the Si/C and Si/C/CNF-1 electrodes. Note that although the Si/C electrode shows a higher second cycle lithium insertion capacity of ca. 1204 mA h g^{-1}, it rapidly drops to 557 mA h g^{-1} after 30 cycles with a retention rate of only 46%. For the Si/C/CNF-1 electrode, the second cycle capacity of 1000 mA h g^{-1} is lower than that of the Si/C electrode, but the retention rate after 30 cycles is as high as 77%. Ji et al. [2] reported that the CNF and nano-Si composite electrode exhibits a high initial lithium insertion capacity of 1100 mA h g^{-1} and a high coulombic efficiency at the first cycle of 82%. However, the retention rate of the lithium insertion capacity was only 57% after 30 cycles. As Si/C/CNF-1 was prepared by the direct mixing of CNF and Si/C, CNF may float mainly on the surface of the Si/C particles, and as a result, CNF may contact directly with the electrolyte, resulting in large initial irreversible capacity from CNF.

The Si/C/CNF-2 composite was also prepared through the other route, where CNF

was covered with pyrolytic carbon derived from PVC. CNF, nano-Si and PVC were mixed and then heated, so that nano-Si and CNF were covered with the PVC-derived pyrolytic carbon.

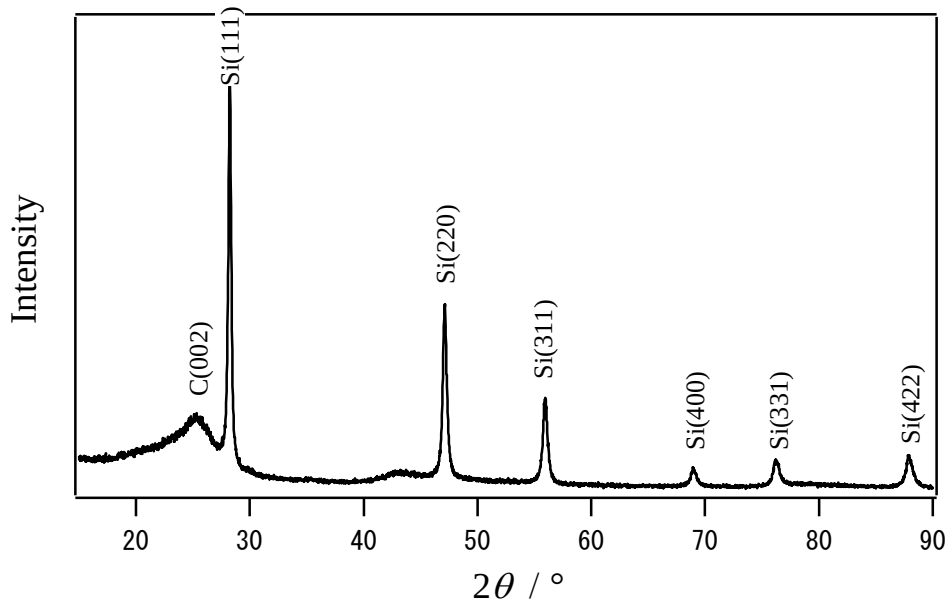

Fig. 3. XRD pattern of Si/C/CNF-2.

Fig. 3 shows an XRD pattern of Si/C/CNF-2 with diffractions of silicon and carbon, but absent of silicon oxide and C-Si alloy diffractions. The broad peak at approximately 25.3º can be attributed to CNF.

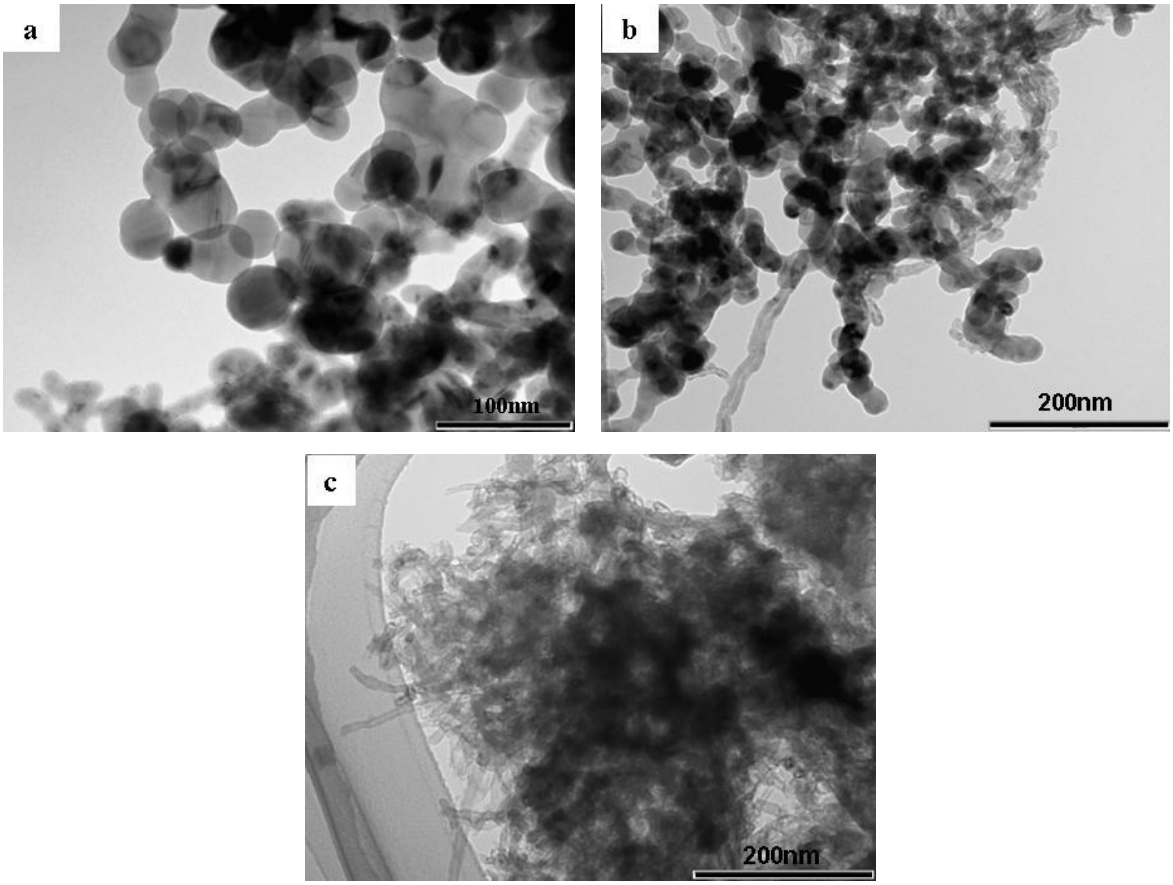

Fig. 4. TEM images of (a) nano-Si powder, (b) Si/CNF mixture, and (c) Si/C/CNF-2.

Fig.4 shows a TEM image of nano-Si, a mixture of nano-Si and CNF, and Si/C/CNF-2. The nano-Si powders are well dispersed in the CNF matrix by ultrasonic mixing in THF, as shown in Fig. 4b. Note that Si/C/CNF-2 has a porous structure (Fig. 4c). The BET surface area of Si/C/CNF-2 is 107.1 $m^2 g^{-1}$, which is significantly higher than that of Si/C/CNF-1. Such a structure offers more free space to buffer the volume changes of Li_xSi during the Li insertion and extraction process [2].

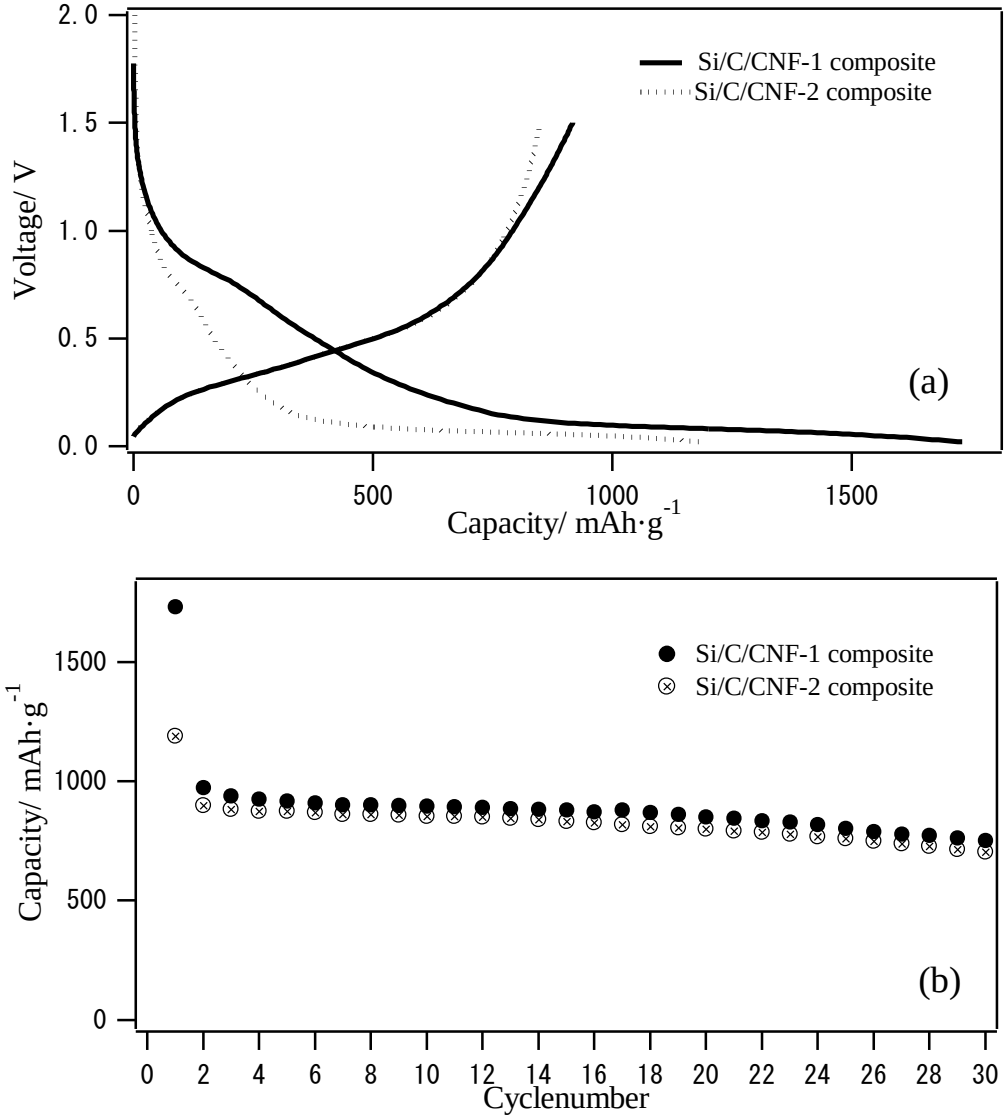

Fig. 5. (a) Voltage vs. lithium insertion capacity curves and (b) cycling performance for Si/C/CNF-1 and Si/C/CNF-2 at room temperature. Current rate 1/10 C; Cut-off voltage 20-1500 mV.

Fig. 5a compares the voltage vs. lithium insertion specific capacity curves for Si/C/CNF-1 and Si/C/CNF-2. Note that Si/C/CNF-2 shows a higher coulombic efficiency of 71%, compared with that of Si/C/CNF-1 (53%). This is due to the covering of the CNF surfaces in Si/C/CNF-2 with the pyrolytic carbon derived from PVC, so that CNF does not directly contact the electrolyte solution. The lithium insertion and extraction cyclic performance of Si/C/CNF-2 is comparable to that of Si/C/CNF-1, as

shown in Fig. 5b. The capacity retention is as high as 78% after 30 cycles. The improved electrochemical performance of the Si/C/CNF-1 and Si/C/CNF-2 composites compared with bare Si/C could be ascribed to the buffering effect of the nanosize CNF matrix, which accommodates the large Si volume expansion and shrinkage during lithium insertion and extraction, which ensures good electronic contact between Si and carbon, imparts many active sites for charge transfer reactions, and preserves the integrity of the electrode structure [2].

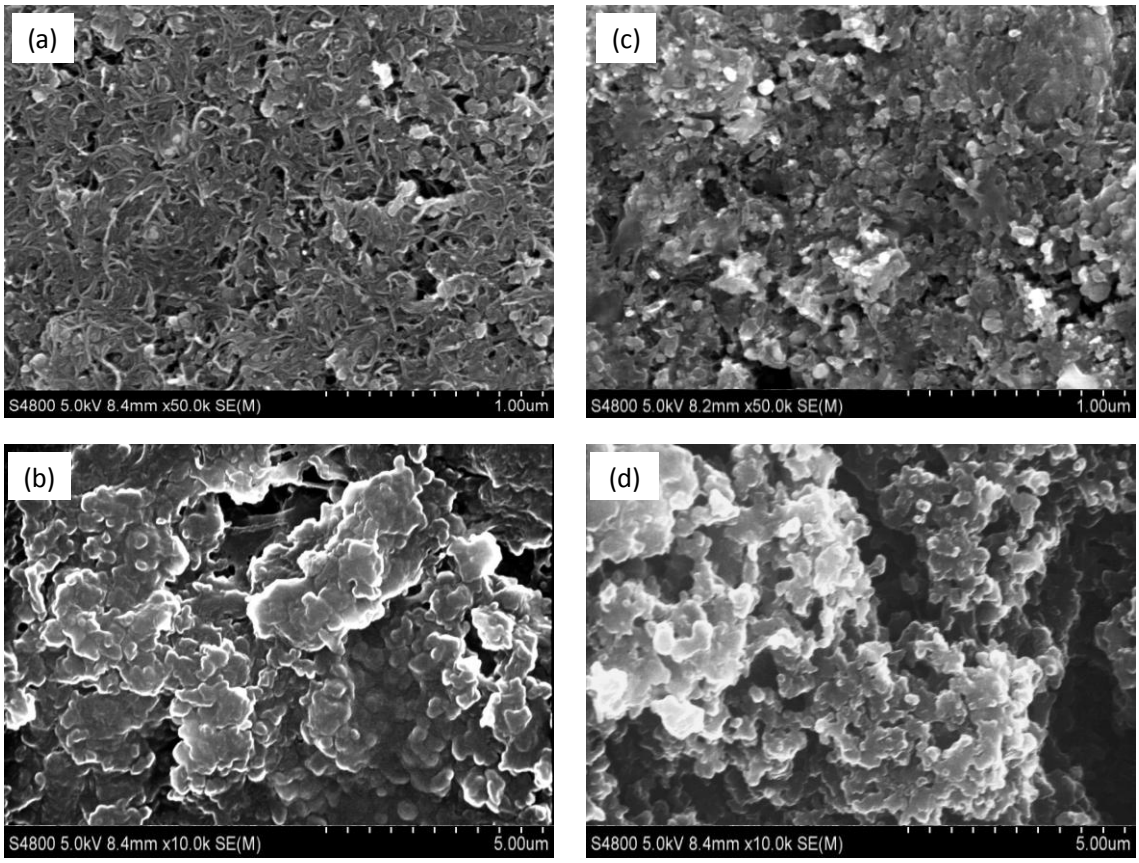

Fig. 6. SEM images of (a) Si/C/CNF-1 before cycling test, (b) Si/C/CNF-1 after 50th lithium insertion and extraction cycle test, (c) Si/C/CNF-2 before cycling test, and (d) Si/C/CNF-2 after 50th lithium insertion and extraction cycle test.

It is important to observe the microstructural changes before and after the cycling tests. Fig. 6 shows SEM images of Si/C/CNF-1 and Si/C/CNF-2 before and after 50 cycles. Fig. 6b shows that the composite Si/C/CNF-1 electrode keeps the homogeneous

surface morphology and shows no obvious cracks even after 50 electrochemical cycles. From figures 6c and 6d, we can see that the porous structure of the Si/C/CNF-2 electrode still remains after cycling. However, the exfoliation of Si/C/CNF-2 from the copper substrate was observed after 20 cycles when a breaker cell was used for measuring the impedance. The impedance profiles of Si/C/CNF-1 and Si/C/CNF-2 before cycling and after 20 cycles are shown in Fig. 7.

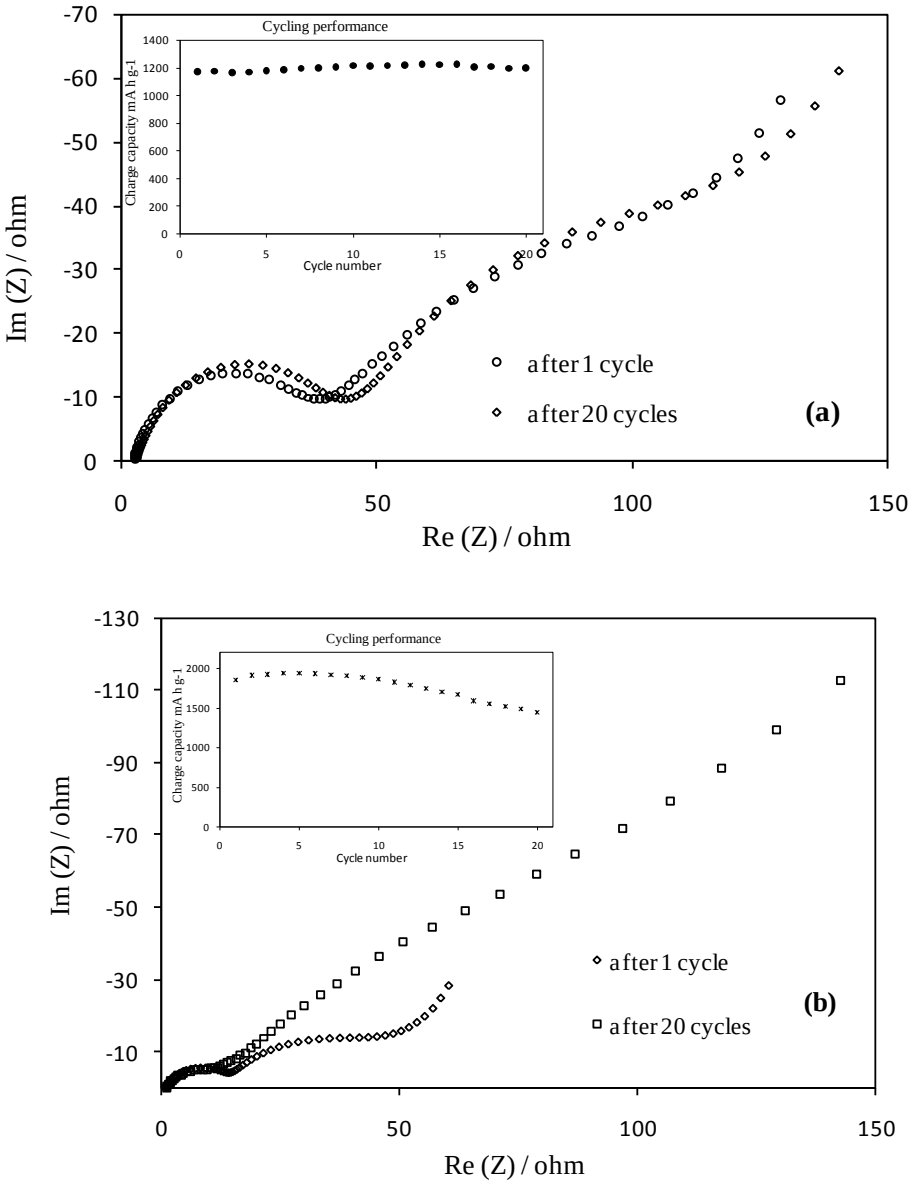

Fig. 7. Impedance profiles for (a) Si/C/CNF-1 and (b) Si/C/CNF-2 after the first and 20th lithium insertion and extraction cycle tests.

The impedance profiles show a semicircle in the high frequency range and a diminished semicircle in the low frequency range. The high frequency semicircle could be attributed to the formation of an SEI caused by the decomposition of the electrolyte solution, and the low frequency semicircle to the charge transfer resistance [7]. Si/C/CNF-1 shows a higher interface resistance from the SEI, which is confirmed by the high irreversible capacity at the first lithium insertion and extraction cycle. No significant change of the impedance profile before and after cycling is observed for Si/C/CNF-1. On the other hand, Si/C/CNF-2 shows a relatively low SEI resistance and a significant increase in the second semicircle by cycling, that is, an increase of the charge transfer resistance by cycling. These results indicate that the active site area for the charge transfer decreases with lithium insertion and extraction cycling. The decrease of in active site area may be due to reduced triple phase boundary between the electrode active material, current collector, and the electrolyte.

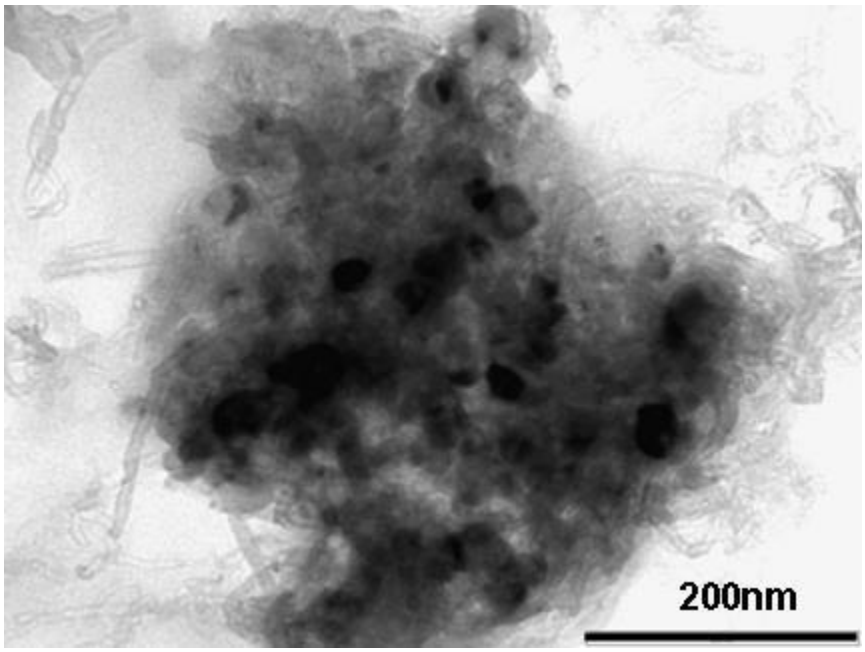

Fig. 8. TEM image of Si/C/CNF-3.

Si/C/CNF-1 showed a high reversible capacity and excellent cycling performance, but a high irreversible capacity was observed at the first lithium insertion and extraction cycle. However, Si/C/CNF-2 exhibited a high reversible capacity and a low irreversible capacity at the first lithium insertion and extraction cycle, but the charge transfer resistance was increased by lithium insertion and extraction cycling. To overcome these weak points of Si/C/CNF-1 and Si/C/CNF-2, a composite electrode of Si/C/CNF-2 and CNF (Si/C/CNF-3) was prepared. Fig. 8 shows a TEM image of Si/C/CNF-3. There is a homogeneous distribution of Si/C/CNF-2 in the CNF matrix.

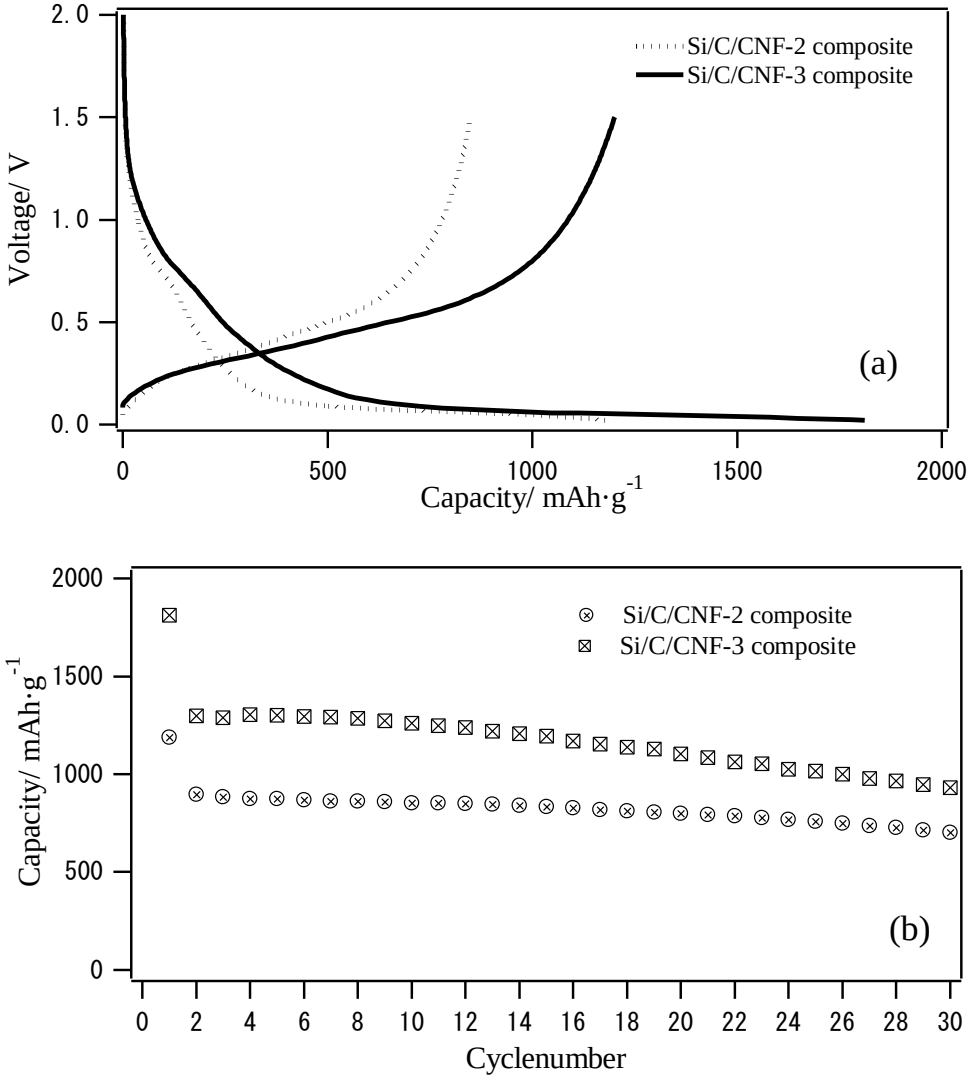

Fig. 9. (a) Voltage vs. lithium insertion capacity curves and (b) cycling performance for Si/C/CNF-2 and Si/C/CNF-3 at room temperature.

The voltage vs. lithium insertion capacity curve and the cyclic performance are shown in Fig. 9 along with that for Si/C/CNF-2, where the lithium insertion and extraction rate was as high as 1/2 C for Si/C/CNF-3 and 1/10C for Si/C/CNF-2. Although Si/C/CNF-3 shows a slightly lower retention rate of 72% compared with 76% for Si/C/CNF-2 after 30 cycles, it exhibits a higher discharge capacity even at a high rate of 1/2 C, compared with that of Si/C/CNF-2 at a 1/10 C rate. After 30 lithium insertion and extraction cycles, Si/C/CNF-3 still maintains a capacity of 931 mA h g^{-1}.

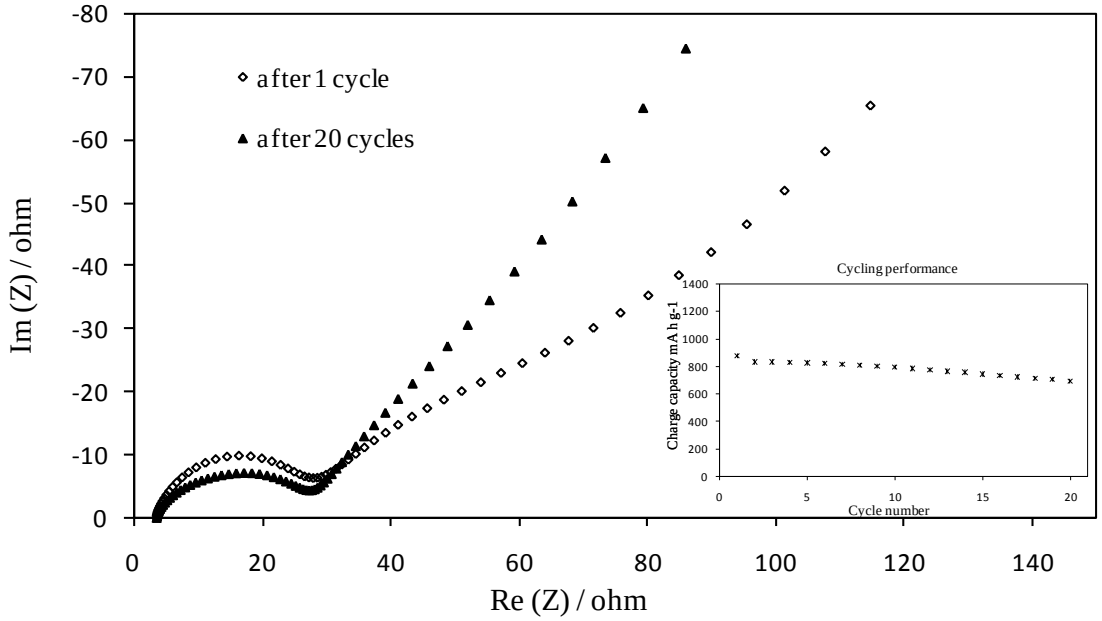

Fig. 10. Impedance profiles for Si/C/CNF-3 after the first and 20th lithium insertion and extraction cycle tests.

Fig. 10 shows the impedance profile change for the Si/C/CNF-3 electrode after the first and 20th lithium insertion and extraction cycle tests. It is quite interesting that the charge transfer resistance of the Si/C/CNF-3 electrode becomes very low by lithium insertion and extraction cycling. The improvement in the electrochemical performance could be attributed to good electrical contact between the active materials, CNF, and the

current collector during the lithium insertion and extraction cycles. This result supports the high rate performance of CNF reported by Subramanian et al. [4].

4. Conclusions

The lithium insertion and extraction performance of nano-Si, carbon, and carbon nano-fiber composite electrodes as lithium electrodes was examined. The composite electrode prepared by mixing carbon-coated nano-Si powder and CNF (Si/C/CNF-1) showed a high reversible capacity and excellent cycling performance, but the first cycle irreversible capacity was high. The composite electrode prepared by heating a mixture of nano-Si, CNF, and PVC (Si/C/CNF-2) showed a high reversible capacity, excellent cyclic performance and low irreversible capacity at the first lithium insertion and extraction cycle. However, a high charge transfer resistance was observed after further lithium insertion and extraction cycles. The best electrode performance was obtained for the composite electrode prepared by mixing Si/C/CNF-2 and CNF. A reversible capacity of 1000 mA h g^{-1} was observed at a high current rate of 1/2 C after 30 lithium insertion and extraction cycles, and a lower irreversible capacity was obtained in the first cycle than that of the Si/C/CNF-1 electrode. High reversible capacity and fairly good cyclability result from utilizing the ductile CNF matrix to buffer the Si volume expansion on the macro domain and maintain good contact with both the active materials and the electrolyte after lithium insertion and extraction cycles.

References:

[1] Q. Si, K. Hanai, N. Imanishi, M. Kubo, A. Hirano, Y. Takeda, O. Yamamoto, J. Power Sources 189 (2009) 761.

[2] L. W. Ji, X. W. Zhang, Electrochem. Commun. 11 (2009) 1146.

[3] H. Habazaki, M. Kiriu, H. Konno, Electrochem. Commun. 8 (2006) 1275.

[4] V. Subramanian, H. W. Zhu, B. Q. Wei, J. Phys. Chem. B 110 (2006) 7178.

[5] L. W. Ji, X. W. Zhang, Electrochem. Commun. 11 (2009) 684.

[6] L.W. Ji, X.W. Zhang, Electrochem. Commun. 11 (2009) 795.

[7] P. J. Zuo, G. P. Yin, Y. L. Ma, Electrochim. Acta 52 (2007) 4878.

1.3 Improvement of cyclic behavior of a ball-milled SiO and carbon nanofiber composite anode for lithium-ion batteries

1. Background

In the 1.2, we proceeded to improve the electrochemical performance of the carbon-coated 50nm-Si anode cast on copper foil, by adding CNF to the carbon-coated 50nm-Si composite in order to improve the electric contact among the copper substrate and the electrode materials. The composites prepared by both methods exhibited high capacity and excellent cycling stability for lithium insertion and extraction. However, when the silicon particle size decreased below 100nm, silicon particles agglomerated very easily during the Li-insertion and extraction, moreover, nanometer silicon powder having a large surface area, showed a large irreversible capacity and reduced the coulombic efficiency because of the increased direct contact with the electrolyte. In the case of SiO, the oxide is irreversibly reduced during the first lithiation process, resulting in the formation of nanosized clusters of amorphous silicon surrounded by Li_2O matrix. After the initial irreversible reaction, lithium reversibly reacts with this amorphous silicon.

We have investigated silicon monoxide powders with different oxygen content (SiO, $SiO_{0.8}$, $SiO_{1.1}$) as anode materials for lithium secondary batteries [1], in which the capacity retention was improved with decreased particle size; however, the capacity fade by cycling became marked with longer cycles. The problem of volume change in Li-alloy is difficult to completely eliminate. Although high specific reversible capacities (above 800mAh g^{-1}) and fairly good cycle life were obtained for nanosize SiO anodes, they had large irreversible capacities (almost 50%) from the formation of Li_2O. From an

application standpoint, there is still considerable room for improvement of the first cycle efficiency and cycle life of such anode systems. In order to remove the large first irreversible capacity, the formation of composites with strong reducing agents such as Li metal powder [2] or lithium nitrides [3] have been effective at the laboratory scale.

Various methods have been reported for improvement of the cycle performance of SiO anodes, especially considering small SiO particles in a matrix. For example, Kim et al. [4] prepared a SiO-carbon composite by ball-milling and pyrolysis. The SiO-carbon composite demonstrated a first coulombic efficiency of 76% and reversible capacity of 710 mAh g^{-1} over 100 cycles. This is attributed to the stable microstructure, enhanced electrical contact afforded by the pyrolyzed carbon, and the amorphous phase transformation of the active material during cycling.

In this study, inexpensive micron size SiO powder was pulverized using high energy mechanical milling (HEMM) and the pulverized SiO was then mixed with CNF. The electrode performance of the SiO/CNF composite anode was investigated as a function of the milling time and was discussed with respect to the change of the Si valence by the milling time. The high irreversible capacity at the first cycle was compensated by chemically precharging with a lithium thin film attached to the composite electrode.

2. Experimental

SiO powder with an average particle size of 8 μm was used as the starting material. The SiO powders were treated by HEMM (Fritsch planetary micro mill) in a zirconia bowl with zirconia balls at a rotational speed of 500 rpm for 6, 12, 24 and 36 h. The SiO powders were placed and sealed in the milling bowl under an Ar atmosphere in a glove

box. The weight ratio of zirconia balls (5 mm diameter) to the SiO powder was maintained at 5:1. The SiO electrodes were prepared as follows. The ball-milled SiO powder was mixed with CNF (Jemco, Japan, 10-20 nm diameter and 0.1-10 μm long) in a 1-methyl-2-pyrrolidone (NMP) solution using a mixer (Thinky, Japan).The weight ratio of SiO to CNF was 70:30. Acetylene black (AB; Denkikagaku, Japan) and polyvinylidene fluoride (PVDF; Kynar, USA) were added into the solution. The weight ratio of SiO/CNF:AB:PVDF was 75:5:20. The slurry of electrode components was cast onto a copper foil and dried at 80 °C for 1 h in open air. The cast electrodes were cut to a size of $1\times1cm^2$. The electrode thickness was in the range of 20-30 μm. The electrodes were further dried at 120 °C under vacuum for 2 h followed by pressing at 200 kgf cm^{-2}. The specific capacity was calculated according to the weight of SiO/CNF. Electrochemical tests of the composite electrodes were conducted using two-electrode coin-type cells (type 2025). The coin-cells were assembled in an Ar-filled glove box using 1 M $LiClO_4$ in an ethylene carbonate (EC) and diethylene carbonate (DEC) mixed solution (1:1 v/v) as the electrolyte and metallic lithium foil (20 μm thick) as the counter electrode. The electrochemical performance of the composite anode was evaluated using a constant current charge-discharge cycling test machine (Nagano BST 2004H, Japan) in the voltage range of 20-1500 mV with a charge-discharge rate of 1/10 C at room temperature. X-ray diffraction (XRD) patterns were obtained using a diffractometer (Rigaku, Rotaflex RU-200B) with Cu Kα radiation. The morphology of the ball-milled SiO powder was examined using scanning electron microscopy (SEM; Hitachi SEM S-4800). Surface area measurements were conducted using a gas absorption analyzer (Shimadzu Micromeritics Tri Star 3000). The change in the chemical structure of the SiO powder by ball-milling was examined by X-ray

photoelectron spectroscopy (XPS) (Shimadzu ESCA 3400) analysis of the Si 2p values.

3. Results and discussion

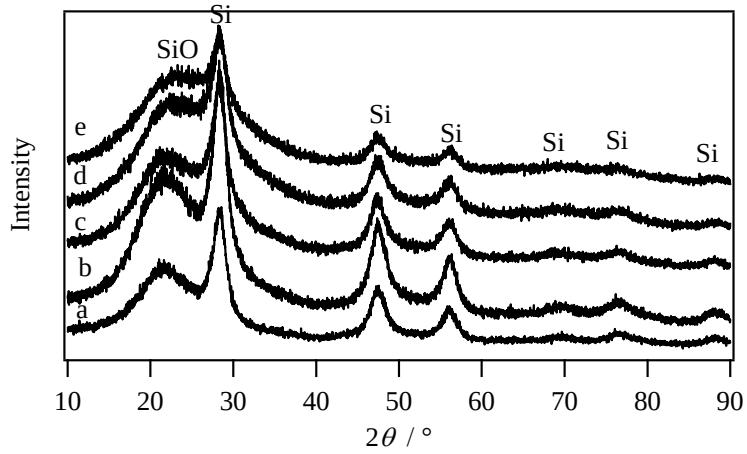

Fig. 1. XRD patterns of (a) as-received SiO and SiO ball-milled for (b) 6, (c) 12, (d) 24, and (e) 36 h.

Fig. 1 shows XRD patterns of the as-received and ball-milled SiO powder, which are similar to that for nanosize $SiO_{1.1}$ (average particle size of 50 nm) reported by Yang et al. [1]. The diffraction peaks of Si and a broad SiO peak were detected in all samples. Ball-milling had no significant effect on the XRD peaks, although a slight decrease of the Si peak height and a slight increase of the SiO peak height were evident. Fig. 2(a-d) shows SEM images of the ball-milled SiO for various milling times and that of the SiO/CNF composite. The initial particle size of 8~10μm was reduced to 0.1~0.4 μm by ball-milling and the BET surface area of the as-received SiO (4.8 m^2 g^{-1}) was increased to 19.5 m^2 g^{-1} by ball-milling for 36 h. The particle size gradually decreases and equals with ball-milling treatment; the main particle size of SiO ball-milled for 12 h is between 0.1~1.0 μm and that for 36h is between 0.1~0.4 μm. In the SiO/CNF composites, SiO particles homogeneously distributed in the CNF matrix, where CNFs cover the SiO particles like muskmelon's surface texture as shown in Fig. 2 (e-h).

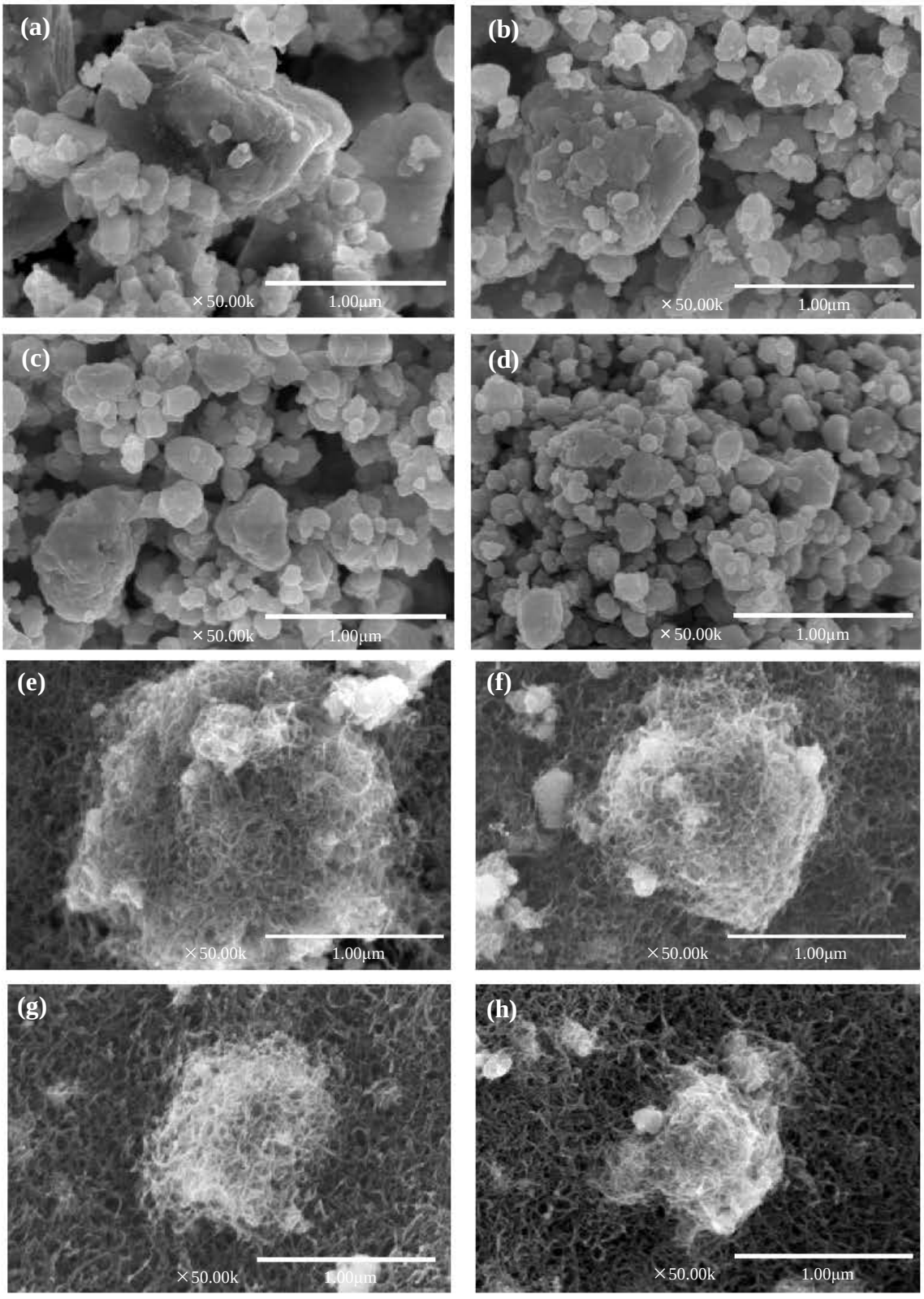

Fig. 2. SEM images of SiO ball-milled for (a) 6h, (b) 12h, (c) 24h, (d) 36 h, and SiO/CNF composites ball-milled for (e) 6h, (f) 12h, (g) 24h, and (h) 36h.

Fig. 3 compares the charge and discharge curves at the first cycle and the cycling stability of the as-received SiO and SiO/CNF composite electrodes at room temperature. The as-received SiO electrode exhibits a similar potential profile to that reported previously [1, 5] in the first lithium insertion (charge) and extraction (discharge), and the observed charge and discharge capacities are 2117 and 1427 mAh g^{-1}, respectively. The high irreversible capacity could be explained by the formation of Li_2O and/or Li_4SiO_4 [5-7];

$$SiO + 2Li = Li_2O + Si, \quad (1)$$

and

$$4SiO + 4Li = Li_4SiO_4 + 3Si \quad (2)$$

Miyachi et al. [6] estimated from XPS analysis that 60% of SiO is converted to Li_2O and lithium silicate. The fine Si particles produced by this conversion reaction react with Li to make an alloy;

$$Si + 4.4\ Li = Li_{4.4}Si \quad (3)$$

The reversible and irreversible capacities calculated from reactions (1) and (3) are 2675 and 1216 mAh g^{-1}, respectively, and those calculated from reactions (2) and (3) are 2006 and 1216 mAh g^{-1}, respectively. The irreversible capacity is calculated to be in a range of 30 to 38%. The observed irreversible capacity of the as-received SiO was estimated to be 33%. These results support the suggested reaction mechanism. The large size SiO particles exhibit a low irreversible capacity and a high reversible capacity at the first cycle; however, the capacity fade by cycling is significant, as shown in Fig. 3(b). We previously reported that the cyclic performance of the Si-C electrode was improved by addition of CNF [8]. The effect of CNF addition to SiO on the electrode performance was examined. The charge capacity of the SiO/CNF composite electrode at the first cycle is almost same as that of SiO. The charge capacity of CNF at the first cycle was

reported to be approximately 660 mAh g^{-1} [8]; therefore, the discharge capacity of SiO in the composite electrode is estimated to be 2760 mAh g^{-1} from the weight of SiO in SiO/CNF (70 wt% SiO in SiO/CNF). The discharge capacity is in good agreement with that calculated from reactions (1) and (3). The charge capacity of 1215 mAh g^{-1} for the SiO/CNF electrode corresponds to 1670 mAh g^{-1} for SiO, where the discharge capacity of CNF was estimated to be 92 mAh g^{-1} [8]. The charge capacity is slightly higher than 1460 mAh g^{-1}calculated from reactions (1) and (3). The difference may be due to an uncertainties in the discharge capacity of CNF and the mass of SiO in the electrode. Figure 3(b) shows that the SiO/CNF composite electrode has better cyclic performance than that observed for the Si-C/CNF electrode [8]. Several factors were considered for the contribution to improved cycling performance by addition of CNF. Firstly, flexible CNFs may function as a good electronic contact, and secondly, the dispersed network of CNFs shown in Fig. 2 (e-h) acts as an effective buffer matrix for the volume change of Li_xSi by cycling [9]. However, the cyclic performance of the as-received SiO and CNF composite electrode is not as good as that of the nanosize SiO electrode reported by Yang et al. [1]. The capacity retention after 50 cycles was only 58%.

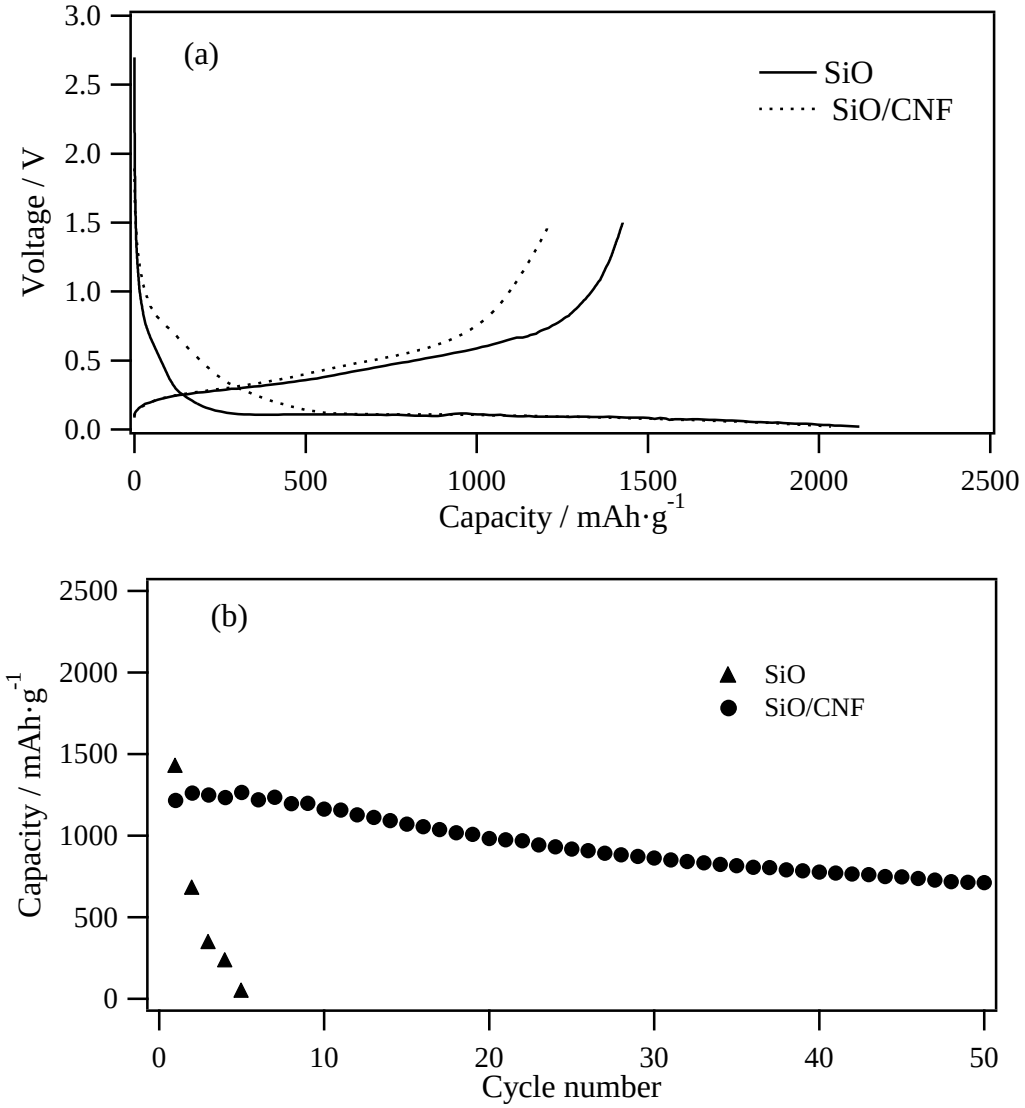

Fig. 3. (a) Charge-discharge curves (1/10 C rate) and (b) cycling performance of the SiO and SiO/CNF electrodes.

On the other hand, the ball-milled SiO/CNF exhibits better charge-discharge cycling performance. The charge-discharge performance for the ball-milled SiO/CNF composite anode at the first cycle, and the change in the discharge capacity by cycling are shown as a function of the ball-milling period in Fig. 4. The best cycling performance is found for the composite SiO/CNF anode with SiO ball-milled for 12 h, where the reversible

capacity is more than 700 mAh g^{-1} and the degradation rate is less than 1% per 100 cycles. The charge and discharge capacities at the first cycle are 2027 and 724 mAh g^{-1}, respectively. The irreversible capacity of the composite anode at the first cycle is as high as 64.3, which may be due to the irreversible reaction of (1) and/or (2) and the electrolyte decomposition observed in the lithium insertion curve in Fig. 4; similar electrolyte decomposition was observed in nanosize SiO [1].

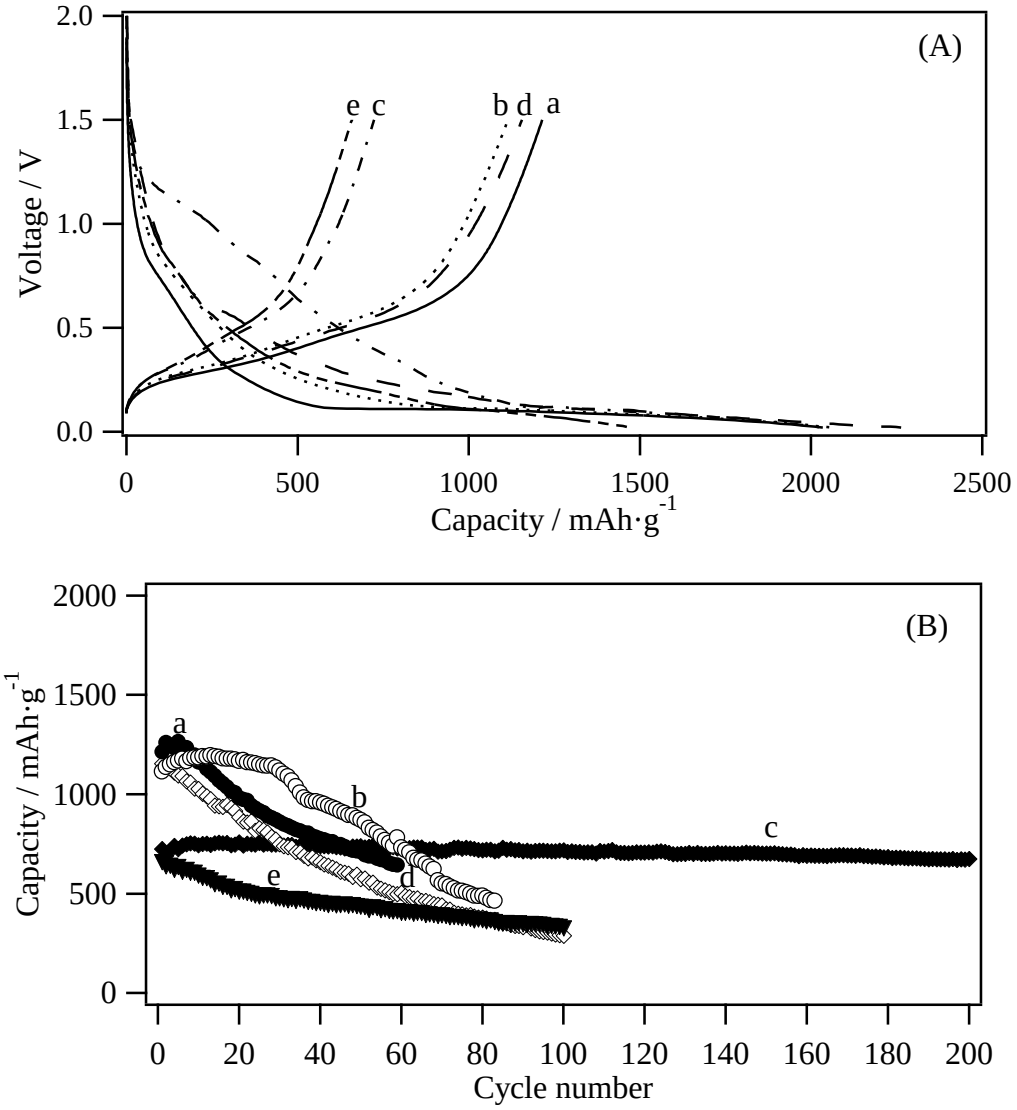

Fig. 4. (A) Charge-discharge curves (1/10 C rate) and (B) cycling performance for SiO/CNF electrode prepared from(a) as-received SiO, and SiO ball-milled for (b) 6, (c) 12, (d) 24, and (e) 36 h.

Fig. 4 shows that ball-milling of the SiO powder has a significant influence on the lithium insertion and extraction performance. SiO is composed of Si and silicon sub-oxides with various valence states [6, 7]. The valence state of Si on the surface for the ball-milled samples was examined using XPS. Typical Si 2p spectra are shown in Fig. 5, where the spectra were obtained after sputtering the SiO surface for 2 h. Each of the spectra was fit to five peaks that correspond to five different Si oxidation states, based on previously reported binding energy values [9]. The spectra in the range of 98 to 106 eV are attributed to Si^0, Si^+, Si^{2+}, Si^{3+} and Si^{4+} from the low energy side, and the ratio of the valence state of SiO was estimated from the area ratio of these spectra. In Table 1, the valence states of ball-milled SiO are given as a function of the ball-milling period. The average valence state of Si on the as-received SiO surface is 2.01, which increases to 3.08 by ball-milling for 36 h. A significant change of the valence state of Si by ball-milling is observed in the decrease of the Si^{2+} state, which could explain the low first cycle capacity for the ball-milled SiO. The conversion reaction from SiO_x to Si may be easier for SiO. However, the excellent cyclic performance for the 12 h ball-milled SiO could not be explained by the change of the valence state of Si, but by the good contact between nanosize SiO and CNF. SiO ball-milled for 24 and 36 h exhibited a large Si^{4+} content; the high resistance of the SiO_2 phase may prevent the formation of conducting paths.

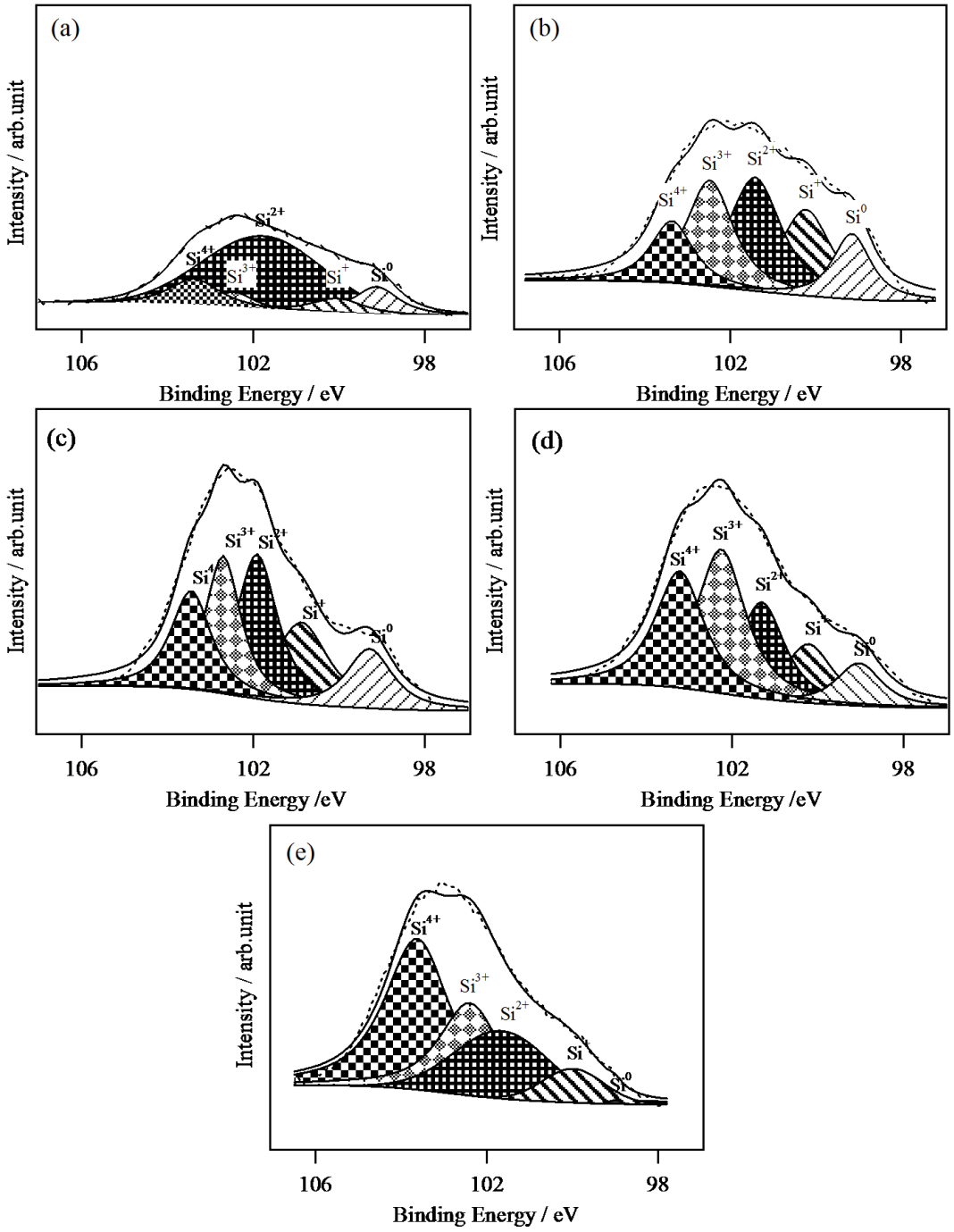

Fig. 5. Si 2p spectra of (a) as-received SiO, and SiO ball-milled for (b) 6, (c) 12, (d) 24, and (e) 36 h.

Table 1 Fraction of the various Si valence states estimated from Si 2p XPS spectra for the ball milled SiO

Milling Time (h)	Fraction of various Si valence states (%)					Average valence of Si
	Si^0	Si^+	Si^{2+}	Si^{3+}	Si^{4+}	
As received	12.1	7.6	61.6	5.8	12.9	2.01
6	12.2	21.7	29.3	24.1	12.7	2.03
12	12.6	20.0	27.2	22.1	18.1	2.13
24	8.9	13.1	20.1	25.9	32.1	2.59
36	0.1	6.9	21.6	26.1	45.3	3.08

Although a high reversible capacity of 675 mAh g^{-1} after 200 cycles was obtained in for the 12 h ball-milled SiO and CNF composite anode, the irreversible capacity was 64.3% at the first cycle, which is undesirable for practical application. Seong and Yoon proposed a new method to compensate the irreversible capacity of SiO using lithium powder [10] and we have reported that the attachment of a lithium thin film to the Si/CNF electrode is effective to reduce the irreversible capacity [11]. In this study, the large irreversible capacity at the first cycle was reduced by attaching a thin lithium sheet to the rim of the composite anode. The amount of lithium sheet calculated from the irreversible capacity was attached to the rim and the test cell was stored at room temperature overnight. The lithium metal reacted with SiO to produce fine Si particles in the CNF matrix (precharge). Fig. 6 shows the first and second cycle charge-discharge curves for the precharged and non-precharged SiO/CNF electrode prepared from SiO ball-milled for 12 h. The irreversible capacity at the first cycle is significantly reduced to 1.9% by precharging and the reversible capacity is slightly increased to 944 mAh g^{-1}. The cycling performance of the precharged and non-precharged 12 h ball-milled SiO/CNF electrode is shown in Fig. 7. A reversible capacity of 890 mAh g^{-1} was

observed after 56 cycles for the precharged 12 h ball-milled SiO/CNF composite electrode, and the capacity retention was as high as 94% for 56 cycles.

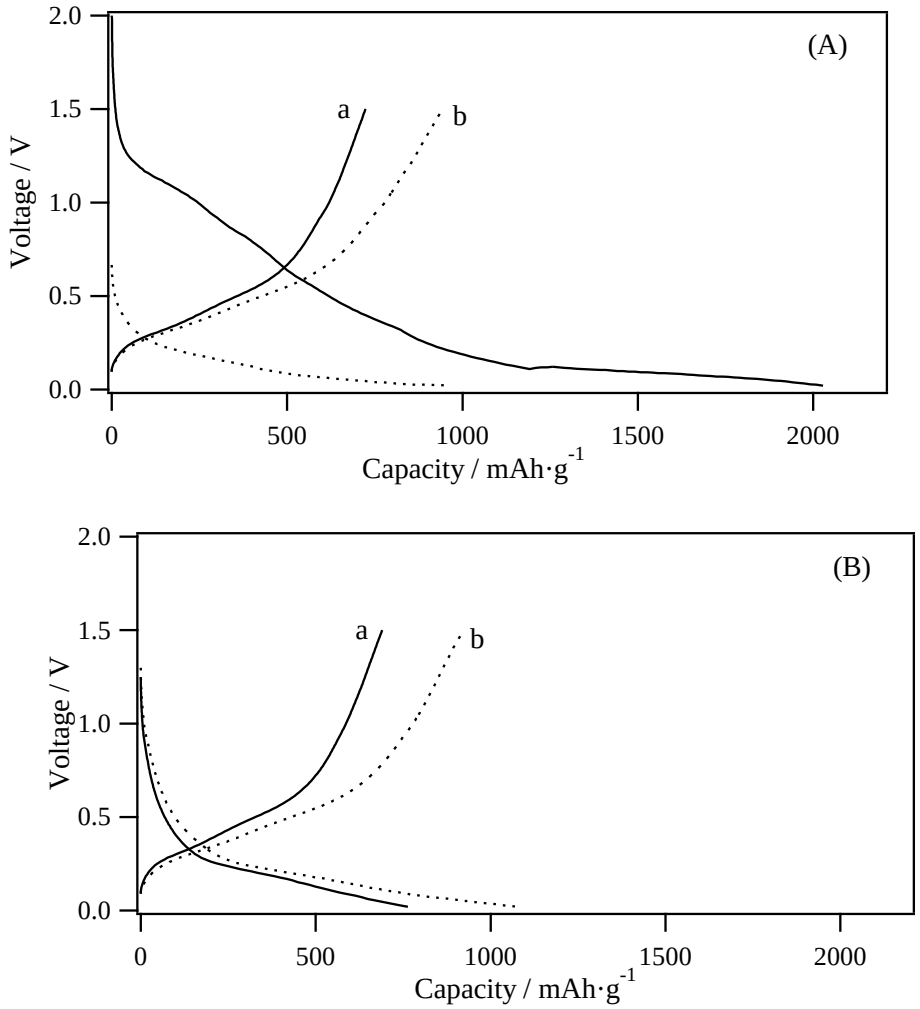

Fig. 6. Charge and discharge curves (1/10 C rate) for the (a) non-precharged and (b) precharged 12 h ball-milled SiO/CNF electrode at the first (A) and second cycles (B).

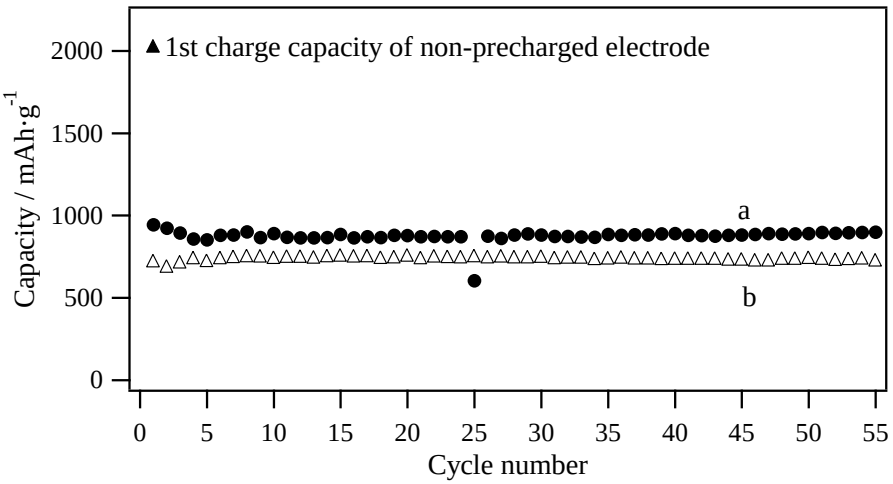

Fig. 7. Discharge capacity (1/10 C rate) vs. cycle number curves of the (a) precharged and (b) non-precharged 12 h ball-milled SiO/CNF electrode.

4. Conclusion

A composite electrode consisting of ball-milled SiO powder and CNF exhibited excellent cycling performance with a high reversible capacity. The best performance was observed for SiO ball-milled for 12 h, which was a mixture of particle sizes from 1 to 0.1 μm. The average valence state of Si in the 12 h ball-milled SiO was 2.13 and the content of Si^{2+} and Si^{4+} were 27.2 and 18.1%, respectively. The excellent cycle performance could be explained by the presence of nanosized SiO and a low content of SiO_2. However, the 12 h ball-milled SiO had high irreversible capacity at the first cycling. The irreversible capacity was reduced to 2% by attachment of a lithium thin film to the electrode, and excellent cycling performance with a high reversible capacity of approximately 900 mAh g^{-1} was observed.

References:

[1] J. Yang, Y. Takeda, N. Imanishi, C. Capiglia, J. X. Xie, and O. Yamamoto, Solid State Ionics, 152/153 (2002) 125.

[2] C. R. Jarvis, M. J. Lain, M. V. Yakovleva, and Y. Gao, J. Power Sources, 162 (2006) 800.

[3] Y. Takeda, J. Yang, and N. Imanishi, Solid State Ionics, 152/153 (2002) 35.

[4] J. H. Kim, H. J. Sohn, H. Kim, G. Jeong, and W. Choi, J. Power Sources, 170 (2007) 456.

[5] M. Miyachi, H. Yamamoto, and H. Kawai, J. Electrochem. Soc., 154 (2007) A376.

[6] M. Miyachi, H. Yamamoto, H. Kawai, T. Ohta, and M. Shirakata, J. Electrochem. Soc., 152 (2005) A2089.

[7] Y. Nagao, H. Sakaguchi, H. Honda, T. Fukunaga, and T. Esaka, J. Electrochem. Soc., 151 (2004) A1572.

[8] Q. Si, K. Hanai, T. Ichikawa, A. Hirano, N. Imanishi, Y. Takeda, and O. Yamamoto, J. Power Sources, 195 (2010) 1720.

[9] G. Hollinger and F. J. Himpsel, Appl. Phys. Lett., 44 (1984) 93.

[10] I. W. Seong and W. Y. Yoon, J. Power Sources, 195 (2010) 6143.

[11] Q. Si, K. Hanai, T. Ichikawa, A. Hirano, N. Imanishi, O. Yamamoto, and Y. Takeda, J. Power Sources, 196 (2011) 6982.

Part 2: Carbon coated nano-Si composite with CNF electrode in the PEO electrolytes.

In part 2, we described the carbon coated nano-Si composite with CNF electrode in PEO electrolytes. We have reported the excellent cycling performance of an amorphous carbon-coated Si anode with CNF (referred to as Si/C@CNF) in liquid electrolyte in Part 1. However, the composite has high irreversible capacity in the first cycle. In the part 2, we focus our attention on the electrochemical behavior of lithium insertion into and extraction from the Si/C@CNF composite electrode in PEO-based electrolytes. We introduced a lithium metal sheet into the Si/C@CNF electrode in an attempt to compensate the first irreversible capacity that resulted in a high initial coulombic efficiency.

2.1. High performance Si/C@CNF composite anode for solid-polymer lithium-ion batteries.

2.1 High performance Si/C@CNF composite anode for solid-polymer lithium-ion batteries

1. Background

Li-ion batteries are one of the great successes from the application of advanced materials and electrochemistry to modern energy storage devices. The energy density for small size batteries of this type is as high as 200 Wh kg^{-1}. In recent years, higher energy density batteries of larger size have been required for applications such as hybrid electric vehicles (HEVs), electric vehicles (EVs) and load leveling devices. However, a battery device with higher energy density also includes a higher risk of fire or explosion. From this point, safety performance is an important issue for applications of lithium-ion batteries. An all-solid state battery that employs a nonflammable solid polymer electrolyte (SPE) may be a reasonable solution to address these safety issues.

Solid-polymer lithium-ion batteries, which have mainly used a lithium metal anode and oxide cathode [1] have been extensively studied for several decades. Although lithium metal anode contributes to a high energy density, it has safety problems arising from dendrite formation on the anode surface [2]. Graphite anodes have exhibited excellent electrochemical performance and good safety performance in ethylene carbonate based electrolyte. Therefore, graphite and related carbon materials have been widely used as the anode in lithium-ion batteries, and the study of graphite in solid-polymer electrolyte have been intensively investigated in recent years. We have previously reported the improved reversibility of a graphite anode with a polymer electrolyte by surface modification of the graphite [3]. This approach enabled the active control of the solid electrolyte interface (SEI) from the graphite surface.

On the other hand, silicon is a most promising material for such applications, due to its high theoretical capacity (4200 mAh g^{-1}) [4]. However, large volume changes occur in Si during Li-insertion and extraction, which causes pulverization of the active materials followed by a loss of electrical contact. As a result, the Si electrode shows a rapid capacity fade [5,6]. One of the most promising methods to solve this problem is to disperse Si into a carbon matrix [7-9], in which the carbon phase acts as both a structural buffer and an electrochemically active material. Other silicon-based anode materials have been synthesized and investigated [10-14]. Liu et al. reported that the combination of a SiO/$Li_{2.6}Co_{0.4}N$ composite electrode in solid poly(ethylene oxide) (PEO) electrolyte resulted in a high first cycle efficiency of ca. 100%; however, the reversible capacity was low as ca. 500 mAh g^{-1} [10]. Kobayashi et al. [11] reported the combination of graphite or SiO/graphite with a SPE. The reversible capacities were 360 mAh g^{-1} for graphite and 1000 mAh g^{-1} for SiO/graphite and the retention was 75% at the 250^{th} cycle versus the initial capacity for graphite, and 72% at the 100^{th} cycle for SiO/graphite. However, the SiO/graphite electrode shows a lower first cycle efficiency with a SPE.

We have previously reported the excellent cycling performance of an amorphous carbon-coated Si anode with carbon nanofiber (CNF) (referred to as Si/C@CNF) in liquid electrolyte [15]. However, the composite has high irreversible capacity in the first cycle. In this study, we focus our attention on the electrochemical behavior of lithium insertion into and extraction from the Si/C@CNF composite electrode in PEO-based electrolytes. We have introduced a certain amount of lithium metal sheet into the Si/C@CNF electrode in an attempt to compensate the first irreversible capacity that results in a high initial coulombic efficiency (referred to as a “precharged electrode”).

2. Experimental

Nano-Si powder (particle size 50 nm, purity >98%) and polyvinyl chloride (PVC) were purchased from Aldrich. CNF (diameter: 10-20 nm, length: 0.1-10 μm) was purchased from Jemco, Japan. The nano-Si/carbon composite (Si/C) was prepared according to the previously reported method [7]. Si particles are surrounded by and embedded in the amorphous porous carbon formed by the thermal decomposition of PVC. The Si/C weight ratio was confirmed to be almost 1:1 from chemical analysis. The Si/C@CNF electrode material was prepared according to the previously reported method [15]. The Si/C composite was mixed with CNF (Si/C:CNF=3:1 in weight) in 1-methyl-2-pyrrolidone (NMP) solution using a rotation mixer. The working electrode was prepared from a mixture of the active materials and poly (vinylidene fluoride) (PVDF) with a Si/C@CNF:PVDF ratio of 80:20 by weight. The mixtures of the electrode components in NMP were uniformly painted onto copper foils, and dried at 80 °C for 1 h. The painted electrodes were cut to a size of 1×1 cm^2 and further dried at 120 °C under vacuum for 2 h, followed by pressing at 200 kgf cm^{-2}. The precharged electrode was prepared by attaching a thin lithium sheet onto the rim of the Si/C@CNF electrode surface. The specific capacity was based on the weight of Si/C.

The PEO-based polymer electrolyte was prepared as follows: PEO (Aldrich, average molecular weight: 6×10^5) and $Li(CF_3SO_2)_2N$ (LITFSI, Fluka) were dissolved in acetonitrile (AN) with Li/O at a molar ratio of 1/18. The polymer electrolyte solution was cast into a polytetrafluoroethylene (PTFE) dish under an Ar atmosphere. After evaporation of the AN at room temperature, the formed film was dried at 110 °C for 12 h under vacuum. Prior to construction of the laminate cell, the combined active material and PEO sheet were preheated at 80 °C for 3 h and then charged and discharged at

60 °C in the voltage range of 0.02-1.5 V using a Nagano BTS 2004H battery cycler. The resulting film thickness was approximately 300 μm. The entire system, Cu/active material/PEO sheet/Li/Cu, was then sealed into a laminate cell for electrochemical testing. The charge and discharge rates were typically set at C/10. The morphology of the electrode was examined using scanning electron microscopy (SEM; Hitachi S-4800). Cyclic voltammograms (CVs) were measured using an automatic polarization system (Hokuto Denko HSV-110). Differential scanning calorimetry (DSC; Rigaku Thermo Plus 8330) measurements were conducted using samples of electrode and electrolyte mixtures packed and sealed in a stainless steel pan under an Ar atmosphere at a scanning rate of 3 °C min^{-1} and with Al_2O_3 as a reference.

3. Results and Discussion

To suppress instability of the electrode morphology upon Li insertion and extraction, nano-Si can be dispersed within an inert matrix containing pyrolytic carbon and CNF.

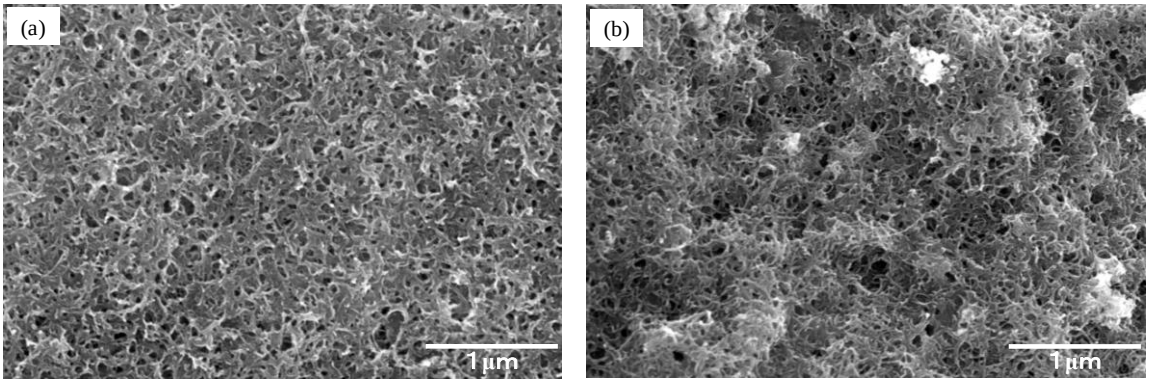

Fig. 1. SEM images of (a) CNF, and (b) the Si/C@CNF

Fig. 1 shows SEM images of CNF (Fig. 1a) and the Si/C@CNF composite (Fig. 1b). Si/C mixed with CNF in NMP is uniformly dispersed in the tangled CNF net. The

Si/C@CNF composite electrode was approximately 60-70 μm thick with the active material loaded at 0.5-0.7 mg cm^{-2}. The charge–discharge characteristics of the Si/C@CNF anodes with a liquid electrolyte of 1 M $LiClO_4$ in ethylene carbonate and diethylene carbonate (EC/DEC, 1:1 vol%) and the PEO-based electrolyte as a solid electrolyte are shown in Fig. 2. The operation temperature was fixed at room temperature for the liquid electrolyte cells and at 60 °C for the PEO-based electrolyte cells. Although the temperatures for these cells were different, they provide a baseline for practical application of such cells under appropriate conditions for the respective electrolytes to exhibit sufficient conductivity.

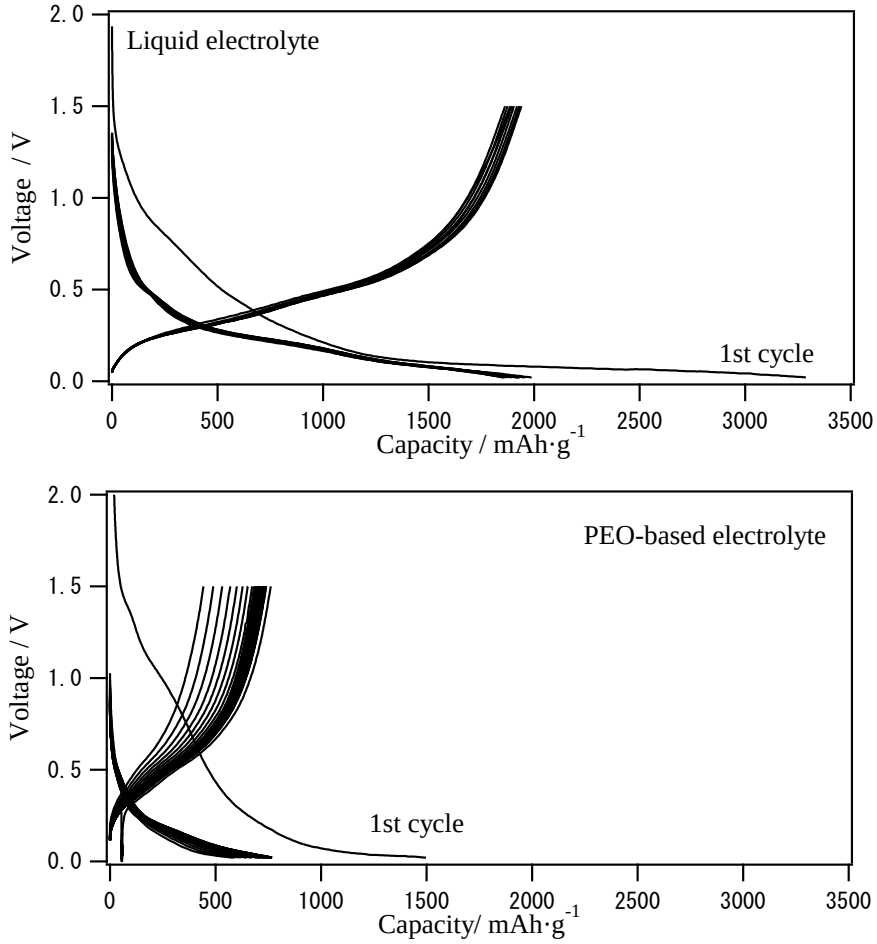

Fig. 2. Charge–discharge curves of the Si/C@CNF composite electrode with a liquid electrolyte (EC-DEC-LiClO4) at room temperature and with the PEO-based electrolyte (PEO-Li(CF3SO2)2N) at 60 °C.

The Si/C@CNF electrode shows a high reversible capacity of ca. 2000 mAh g^{-1} in the liquid electrolyte from the second cycle. In contrast, the cell with PEO-based electrolyte exhibits a smaller capacity of ca. 500 mAh g^{-1}. However, the cycling performance of the PEO-based electrolyte cell in Fig. 3 shows an increase in capacity with the cycle number with a cycling efficiency of almost 97%.

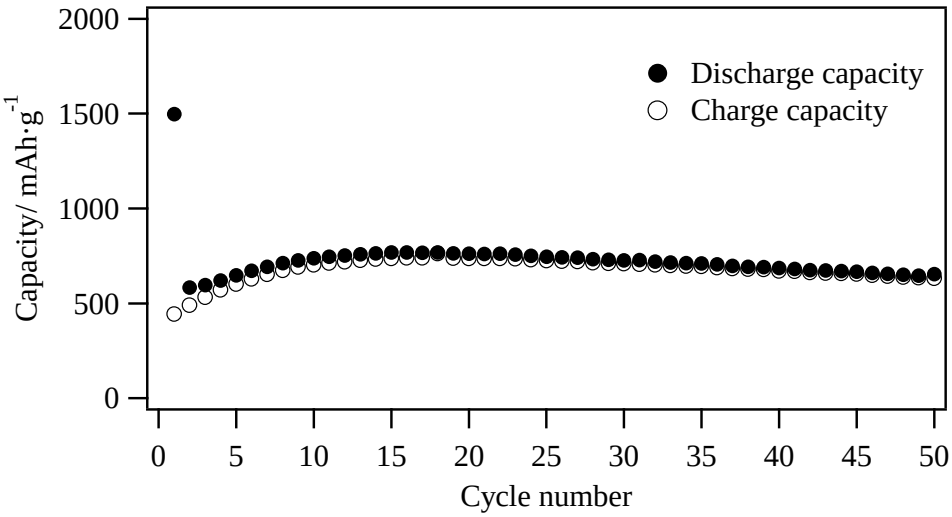

Fig. 3. Cycling performance of the Si/C@CNF electrode with the PEO-based electrolyte at 60 °C. The thickness of the Si/C@CNF electrode was ca. 70 μm.

The lower capacity of the PEO based cell compared with the liquid electrolyte cell is explained by the small active contact area between the electrode and electrolyte. The Si/C@CNF electrode in this study contains no PEO-based electrolyte. Typically, the electrolyte is also mixed with the active electrode materials for preparation of an all-solid state cell. We prepared electrodes with various combinations of the PEO electrolyte and active materials; however, no suitable performance was obtained. Therefore, in order to reduce the lithium diffusion length, a thinner electrode was prepared and the performance was examined. Heat treatment of the electrode/PEO electrolyte system was also performed at 80 °C with the expectation that the PEO

electrolyte would infiltrate into the electrode. The electrochemical performance of heat-treated (80 °C) anode with the PEO-based electrolyte at 60 °C is shown in Fig. 4, where the thickness of the Si/C@CNF electrode was approximately 30 μm, and the loaded active material was 0.2 mg cm^{-2}. The reversible capacity was enhanced to 2151 mAh g^{-1} in the second cycle, which is almost comparable to that for the liquid electrolyte system. This result implies that even in a polymer electrolyte system, an increase of the contact area between the active material and the electrolyte can increase the utilization of the active material. The graphite anode for the solid polymer lithium battery also exhibited similar behavior [3,16]. Unfortunately, the capacity fade is much larger than that for the liquid electrolyte, and this will be discussed later.

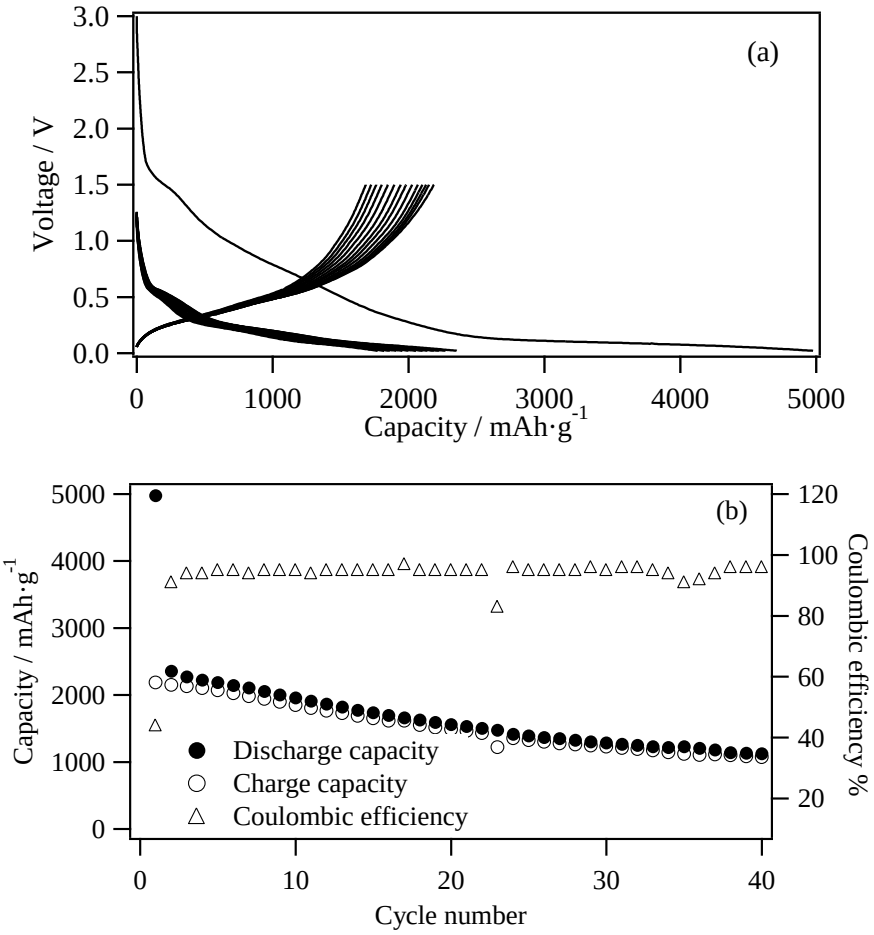

Fig. 4. (a) Charge and discharge curves and (b) cycling performance of the Si/C@CNF thin electrode with the PEO-based electrolyte at 60 °C. The thickness of the Si/C@CNF electrode was ca. 30 μm.

Another problem for the Si/C@CNF electrode with the PEO-based electrolyte cell is the low initial coulombic efficiency, which was as low as 44%. The Si/C@CNF electrode also showed a low initial coulombic efficiency of 58% in the liquid electrolyte. This can be attributed to irreversible Li-Si alloy formation, the electrochemical reduction of electrolyte on the anode surface, and the large irreversible capacity of CNF itself.

Jarvis et al. reported a pre-lithiation method using lithium metal powder to reduce the first irreversible capacity [17]. In the present study, a precharged electrode was realized by placing a thin lithium sheet onto the Si/C@CNF electrode surface. As shown in Fig. 4, the irreversible capacity of the original electrode in the 1st cycle was approximately 2490 mAh g^{-1}. The weight of the active material in the original electrode was 0.2 mg; therefore, the irreversible capacity was approximately 0.498 mAh. The weight of lithium metal was calculated on the basis of the amount of irreversible capacity and was approximately 0.13 mg. The actual amount of lithium added was approximately 0.15 mg.

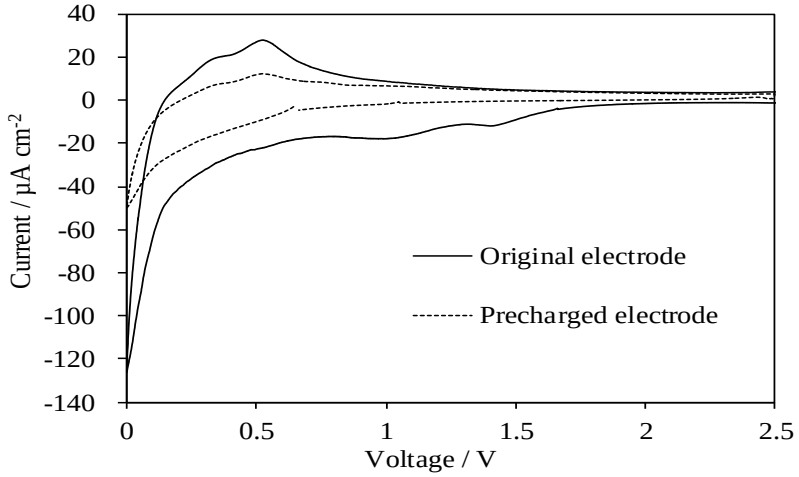

Fig. 5. Cyclic voltammograms (CVs) of the original and precharged electrodes with PEO-based electrolyte for the first cycle. The voltage was scanned in the range of 0-2.5 V at a scan rate of 0.017 mV s^{-1}.

Fig. 5 shows cyclic voltammograms for the original and precharged electrodes with the PEO-based electrolyte for the first cycle measured between 0 and 2.5 V at a scan rate of 0.017mV s^{-1}. Three current peaks appear for the non-precharged electrode (original electrode) at potentials of 1.4, 1.0, and 0 V in the first reduction half-cycle (lithium insertion). The potentials of the two former peaks may correspond to (1) the reductive decomposition of the electrolyte and the subsequent formation of the SEI film on the surface of the active particles, and (2) lithium insertion into the CNF structure, from which the lithium ions are not extracted in the following charge process. In the CV profile of the precharged electrode, only a peak at around 0.5-0 V was observed in the first reduction sweep, which indicates the formation of Li-Si alloys. Side reactions observed in the original electrode are already completed prior to the CV measurements. In the following half-cycle (Li extraction), two broad peaks appear at around 0.3 and 0.55 V in both electrodes, representing two Li extraction stages, which correspond to silicon, disordered carbon and the CNF.

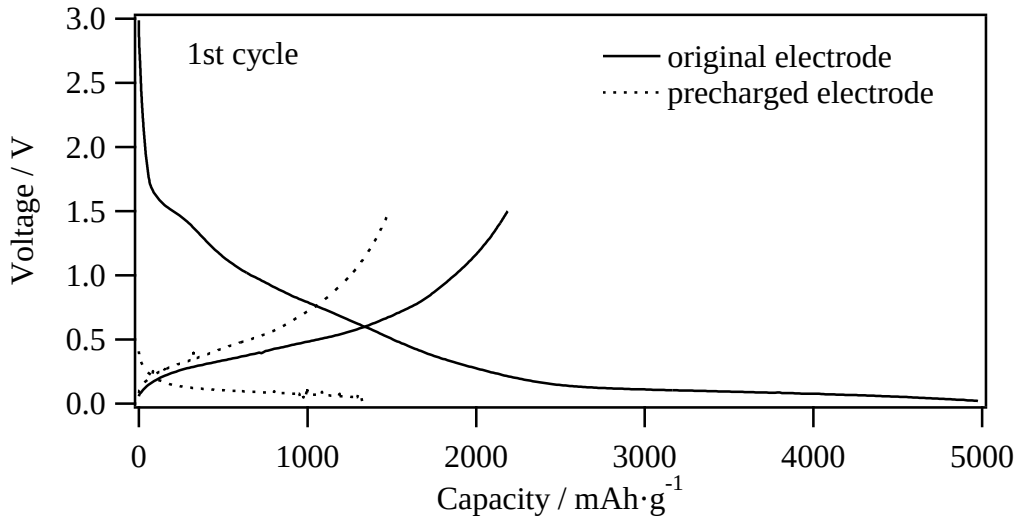

Fig. 6. Charge and discharge curves of the original and precharged electrodes with the PEO-based electrolyte at 60 °C in the first cycle.

Fig. 6 shows the voltage profiles of both the original and precharged electrodes in the first cycle with the PEO-based electrolyte. The original electrode had an initial potential of 3.00 V, whereas that of the precharged electrode was 0.41 V. The decrease in potential means that an amount of lithium metal reacts with the compounds and is attributable to the irreversible capacity, as indicated in Fig. 5. Consequently, this improves the coulombic efficiency of the precharged electrode. The discharge capacity of the original electrode was 4976 mAh g^{-1}, whereas that following the first charge capacity was 2187 mAh g^{-1}, so that the coulombic efficiency was only 44%. On the other hand, the first discharge capacity of the precharged electrode was only 1324 mAh g^{-1} while the charging capacity was 1484 mAh g^{-1}, which indicates a coulombic efficiency of 112% (The coulombic efficiency of >100% is due to the excess lithium added, because it was difficult to adjust exactly such a small amount of Li metal). Therefore, the lithium sheet functioned well as a reducing agent for the Si/C@CNF electrode during cycling of the battery.

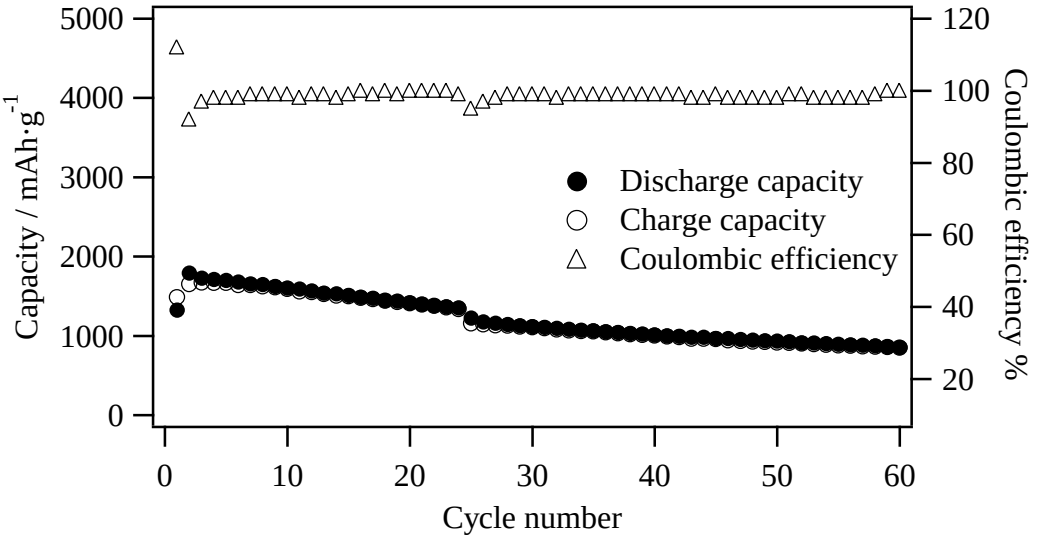

Fig. 7. Cycling performance of the precharged electrode with the PEO-based electrolyte at 60 °C.

Fig. 7 shows the specific capacities and coulombic efficiencies of the precharged electrode as a function of the cycle number. As shown in Fig. 6, the first discharge and charge capacities of the precharged electrode were 1324 and 1484 mAh g^{-1}, respectively, of which the values are lower than the returned capacity(2186 mAh g^{-1}) in the first cycle of the original electrode (Figs. 4b and 6). This may be attributed to the initial inhomogeneous electrode surface caused by attachment of the Li sheet. After several cycles, the capacity in the precharged electrode becomes almost comparable to that in the original electrode (see Table 1). From this point, the lithium metal added has little relation to the reversibility, but is only effective to reduce the first irreversible capacity.

Table 1 Cycle performance of the original and precharged electrodes.

Cycle number	Original electrode			Precharged electrode		
	Charge Capacity (mAh g^{-1})	*Discharge capacity (mAh g^{-1})*	*Coulombic efficiency (%)*	*Charge Capacity (mAh g^{-1})*	*Discharge capacity (mAh g^{-1})*	*Coulombic efficiency (%)*
1st	2186	4676	43.94	1484	1324	112.15
2nd	2151	2354	91.37	1651	1791	92.17
3th	2128	2272	93.65	1670	1726	96.77
10th	1848	1956	94.49	1589	1601	99.21
20th	1486	1559	95.33	1411	1412	99.94
30th	1226	1285	95.47	1106	1116	99.13
40th	1073	1122	95.64	1002	1008	99.31

The cycle performance of the original and precharged electrodes is compared in Table 1. After 40 cycles, the capacity of both electrodes is approximately half of the original, which is in contrast to the case of the liquid electrolyte (Fig. 2). This is attributed to many causes; detachment of the particles in the electrode, due to the large

volume change of Si during the cycling, the formation of reaction products from decomposition of the polymer contacting the electrode, and the formation of inactive Si-Li alloys by the insertion of a large amount of Li. When the lower cut-off voltage during cycling is less than 0.05 V, it is known that the crystalline $Li_{15}Si_4$ phase appears, from which Li is cannot be easily extracted [18]. However, in the present work, the formation of the crystalline $Li_{15}Si_4$ phase was not observed, but only the amorphous phase remained even with a cut-off voltage of 0.02 V, according to XRD observations. The Si powder used was nanosize silicon (50 nm), and Hatchard and Dahn reported that the crystalline $Li_{15}Si_4$ phase forms only above a critical size of approximately 2 μm [19]. Therefore, the Si used in the present research is considered to be too small to form the crystalline $Li_{15}Si_4$ phase. The capacity fade with cycling may therefore be attributed to imperfections of the electrode texture. Further optimization of the texture and composition of the Si/C@CNF electrode is expected to result in higher performance of the solid polymer lithium battery.

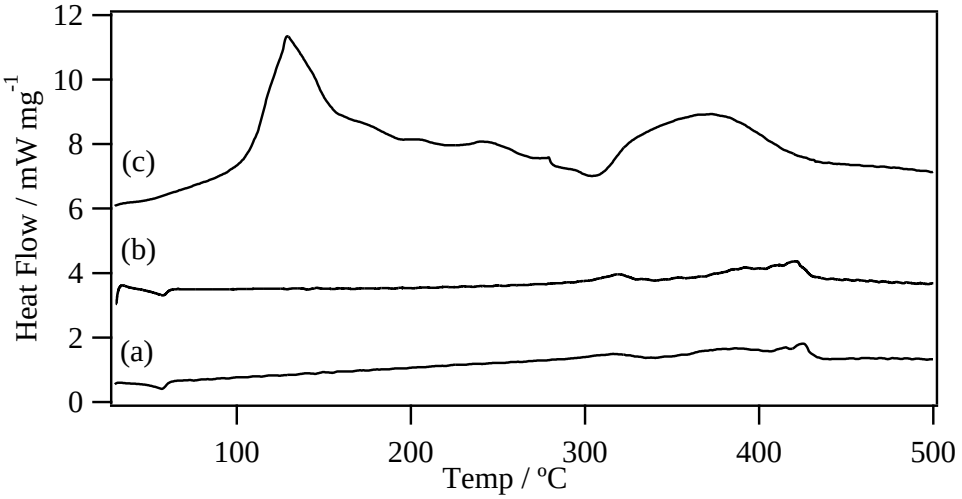

Fig. 8. DSC curves for (a) the original and (b) precharged electrodes with the PEO-based electrolyte, and (c) the original electrode with a liquid electrolyte of $LiPF_6$ in EC-DEC.

The safety of small-size lithium-ion batteries for conventional applications is well established. In contrast, the safety of large-size lithium-ion batteries is still questionable, especially in the case of abusive use. The safety of lithium-ion batteries is mainly related to the thermal reactivity of the components.

Fig. 8 shows differential scanning calorimetry (DSC) curves for three fully lithiated electrodes; (a) the original electrode with the PEO-based electrolyte, (b) the precharged electrode with the PEO electrolyte, and (c) the original electrode with the liquid electrolyte. Only small broad peaks were observed for both the PEO-based electrolyte samples at temperatures higher than 300 °C, while strong peaks appeared for the liquid electrolyte sample from low temperatures of 100 °C. The specific reaction heats for the original and precharged electrodes with the PEO-based electrolyte were 35.7 J g^{-1} and 51.2 J g^{-1}, respectively. The values were normalized on the basis of the heat per discharge capacity to 0.024 J mAh^{-1} for the original electrode and 0.034 J mAh^{-1} for the precharged electrode. On the other hand, the specific reaction heat and heat per discharge capacity of the original electrode with the liquid electrolyte were 347.7 J g^{-1} and 0.23 J mAh^{-1}, respectively. This indicates that the solid lithium polymer battery has a large advantage over the liquid electrolyte lithium battery with respect to safety.

4. Conclusions

The lithium insertion and extraction performance of a Si/C@CNF composite electrode for a solid-polymer lithium secondary battery was examined. The electrode showed a high reversible capacity and good cycling performance, although the first cycle irreversible capacity was very high. In order to increase the availability of the

Si/C@CNF anode, a “precharged” method using lithium sheet was applied. The coulombic efficiency of the precharged electrode for the first cycle was as high as 112% and after the third cycle, the lithium insertion and extraction efficiency reached almost 100%. A reversible capacity of more than 1000 mAh g^{-1} was maintained after 40 cycles. The Si/C@CNF electrode with the PEO-based electrolyte was revealed to have suitable safety characteristics for practical application. These results should contribute to the development of silicon-based anode materials for solid-polymer lithium-ion batteries.

References:

[1] M. Gauther, D. Fauteux, G. Vassort, A. Belanger, M. Duval, P. Ricoux, J.M. Chabagno, D. Muller, P. Rigaud, M.B. Armand, D. Deroo, J. Electrochem. Soc. 132 (1985) 1333-1340

[2] C. Brissot, M. Rooso, J.N. Chazalviel, S. Lascaud, J. Power Sources 81-82 (1999) 925-929

[3] N. Imanishi, Y. Ono, K. Hanai, R. Uchiyama, Y. Liu, A. Hirano, Y. Takeda, O. Yamamoto, J. Power Sources 178 (2008) 744-750

[4] C. J. Wen, R. A. Huggins, J. Solid State Chem. 37 (1981) 271-278

[5] C.K. Chan, R. Ruffo, S.S. Hong, R.A. Huggins, Y. Cui, J. Power Sources 189 (2009) 34-39

[6] B.C. Kim, H. Ueno, T. Satou, T. Fuse, T. Ishihara, M. Ue, M. Senna, J. Electrochem. Soc. 152 (2005) A523-A526

[7] Q. Si, K. Hanai, N. Imanishi, M. Kubo, A. Hirano, Y. Takeda, O. Yamamoto, J. Power Sources 189 (2009) 761-765

[8] Y. Liu, K. Hanai, J. Yang, N. Imanishi, A. Hirano, Y. Takeda, Solid State Ionics 168

(2004) 61-68

[9] P.J. Zuo, G.P. Yin, Z.L. Yang, Z.B. Wang, X.Q. Cheng, D.C. Jia, C.Y. Du, Mater. Chem. Phys. 115 (2009) 757-760

[10] Y. Liu, J. Yang, N. Imanishi, A. Hirano, Y. Takeda, O. Yamamoto, J. Power Sources 146 (2005) 376-379

[11] Y. Kobayashi, S. Seki, Y. Mita, Y. Ohno, H. Miyashiro, P. Charest, A. Guerfi, K. Zaghib, J. Power Sources 185 (2008) 542-548

[12] H.Y. Lee, Y.L. Kim, M.K. Hong, S.M. Lee, J. Power Sources 141 (2005) 159-162

[13] M.S. Park, S. Rajendran, Y.M. Kang, K.S. Hana, Y.S. Hand, J.Y. Lee, J. Power Sources 158 (2006) 650-653

[14] T. Li, Y.L. Cao, X.P. Ai, H.X. Yang, J. Power Sources 184 (2008) 473-476

[15] Q. Si, K. Hanai, T. Ichikawa, A. Hirano, N. Imanishi, Y. Takeda, O. Yamamoto, J. Power Sources 195 (2010) 1720-1725

[16] D. Saito, Y. Ito, K. Hanai, T. Kobayashi, N. Imanishi, A. Hirano, Y. Takeda, O. Yamamoto, J. Power Sources 195 (2009) 6172-6176

[17] C.R. Jarvis, M.J. Lain, M.V. Yakovleva, Y. Gao, J. Power Sources 162 (2006) 800-802

[18] M. N. Obrovac and L. Christensen, Electrochem. Solid-State Lett. **7** (2004) A93-A96

[19] T. D. Hatchard and J. R. Dahn, J. Electrochem. Soc. 151 (2004) A838-A842

Summary

The volume effects of silicon upon Li insertion and extraction can be effectively suppressed by designing a composite microstructure containing ultrafine silicon which is uniformly dispersed in a ductile conducting carbonaceous matrix with electron/ion conductivity. By this way, in the part 1, several types of Si-based composites have been developed by means of pyrolysis process in accompany with adjunction of CNF in the liquid electrolyte. After only the pyrolysis process, obtained Si/C composite shows fairly rapid capacity decay, although the Si/C composite have better capacity retention than only Si during cycling. The pyrolized carbon matrix alone is not sufficient to accommodate the large volume change of silicon during the cycling, which leads to the cracking and crumbling of the Si/C particles. The loss in electronic contact with the Si particles therefore results in the gradual degradation of the electrode. We found that the CNFs homogeneously dispersed on the Si/C mixture surface form a secondary conductive matrix due to the ability of the CNFs to wrap the Si/C particles, thus holding them together and keeping the electronic contact. With the formation of the secondary conductive matrix, these Si particles are kept in contact within two-layer matrixes of the disordered carbon and the CNFs and thus the capacity of the electrode is largely maintained. Moreover, a new type of the composite was also prepared through the other route, where CNF was covered with pyrolytic carbon derived from PVC. CNF, Si and PVC were mixed and then heated, so that Si and CNF were covered with the PVC-derived pyrolytic carbon. The new composite material has a porous structure. Such a structure offers more free space to buffer the volume changes of Li_xSi during the Li insertion and extraction process. However, when the particle size is down to below

100nm, silicon active particles are very easy to reunion during the Li-insertion and extraction to form the electrochemical sintering. Moreover, nanometer silicon powder shows a large surface area, so the increase in direct contact with the electrolyte leads to a large irreversible capacity and reduces the coulomb efficiency. In addition, nanometer silicon powder is produced mainly by the laser method, so the preparation costs are very high. An inexpensive micron size of SiO powder was pulverized using HEMM and then mixed with CNF. The electrode performance of the SiO/CNF composite anode was investigated as a function of the milling time and was discussed with respect to the change of the Si valence by the milling time. The high irreversible capacity at the first cycle was compensated by chemically precharging with a lithium thin film attached to the composite electrode. The SiO was ball-milled for 12 h with CNF to produce a composite electrode material that exhibited excellent cycling performance. A reversible capacity of approximately 700 mAh g^{-1} was observed after 200 cycles. Several factors were considered for the contribution of the improved cycling performance. Firstly, by the micro articulation, the best particle size distribution was obtained for better lithium ion diffusion. Secondly, the flexible CNF may function as a good electronic conductor and formed a good morphology properties effectively acted as a buffering matrix and greatly alleviated the volume changes of Si upon cycling. Finally, the content ratio of Si^{4+} is not too high, which makes it possible to ensure a certain amount of Si^{0} capable of reaction and thus to more reliably hold a capacity.

Solid-state rechargeable lithium ion batteries are principle and promising power sources for a wide variety of electronics. However, graphitic carbon that is currently used as negative electrode material in the commercial Li-ion batteries appears to be unsatisfied due to low theoretic capacity and poor thermal stability under lithiated state.

Therefore, there is even-increasing research in the feasibility of the replacement of graphitic anodes. Part 2 is described the carbon coated nano-Si composite with CNF electrode in PEO (polyethylene oxide) electrolytes. The lithium insertion and extraction performance of a Si/C@CNF composite electrode for a solid-polymer lithium secondary battery was examined. The electrode showed a high reversible capacity and good cycling performance, although the first cycle irreversible capacity was very high. In order to increase the availability of the Si/C@CNF anode, a "precharged" method using lithium sheet was applied. The coulombic efficiency of the precharged electrode for the first cycle was as high as 112% and after the third cycle, the lithium insertion and extraction efficiency reached almost 100%. A reversible capacity of more than 1000mAh g^{-1} was maintained after 40 cycles. The Si/C@CNF electrode with the PEO-based electrolyte was revealed to have suitable safety characteristics for practical application. These results should contribute to the development of silicon-based anode materials for solid-polymer lithium-ion batteries.

Acknowledgment

My heartfelt appreciation goes to Prof. Yasuo Takeda (武田保雄) whose comments and suggestions were of inestimable value for my study. I am also indebt to Prof. Nobuyuki Imanishi (今西誠之), Prof. Tatsuo Horiba (堀場達雄) Prof. Atsushi Hirano (平野敦), Takayuki Ichikawa (市川貴之) and Prof. Osamu Yamamoto (山本治) whose comments made enormous contribution to my work.

I would also like to express my gratitude to Kazuma Hanai (花井一真), thank you for your technical assistance and carefully guide.

I am also greatly indebted to Prof. Michael Brian Phillips and Tao Zhang, who kindly give me a hand when I was writing papers in English.

Last my thanks would go to Astuko Ogura (小倉篤子), Masahiro Ueno (上野雅弘), Ichiro Uechi (上地一朗), who have instructed and helped me a lot in the past years, and many thanks to the students at the エネルギー変換科学講座.

The list of papers and presentations

Papers

[1] Highly reversible carbon-nano-silicon composite anodes for lithium rechargeable batteries

Qin Si, K. Hanai, N. Imanishi, M. Kubo, A. Hirano, Y. Takeda, O. Yamamoto

Journal of Power Sources, 189 (2009) 761-765.

[2] A high performance silicon/carbon composite anode with carbon nanofiber for lithium-ion batteries

Q. Si, K. Hanai, T. Ichikawa, A. Hirano, N. Imanishi, Y. Takeda, O. Yamamoto

Journal of Power Sources, 195 (2010) 1720-1725.

[3] High performance Si/C@CNF composite anode for solid-polymer lithium-ion batteries

Q. Si, K. Hanai, T. Ichikawa, A. Hirano, N. Imanishi, O. Yamamoto, Y. Takeda

Journal of Power Sources, 196 (2011) 6982-6986.

[4] Improvement of cyclic behavior of a ball-milled SiO and carbon nanofiber composite anode for lithium-ion batteries

Q. Si, K. Hanai, T. Ichikawa, M. B. Phillipps, A. Hirano, N. Imanishi, O. Yamamoto, Y. Takeda

Journal of Power Sources, 196 (2011) 9774-9779.

[5] カーボンナノファイバーを用いたリチウム二次電池用新規Si／C複合負極材料

斯 琴，花井 一真，平野 敦，今西 誠之，山本 治，武田 保雄

粉体および粉末冶金第 57 巻第 11 号 （2010）734-740.

Presentations

14th International Meeting On Lithium Batteries (IMLB) (2008/6/22-2008/6/28)

Si/CPE-carbonized Composite Anode for Li-ion Batteries

Q. Si, K. Hanai, N. Imanishi, A. Hirano, Y. Takeda, O.Yamamoto

Asian Collaborative Forum for Women Researchers in Science and Technology (2008/12/20)

Highly reversible carbon-nano-silicon composite anodes for lithium rechargeable batteries

Q. Si, K. Hanai, N. Imanishi, A. Hirano, Y. Takeda, O.Yamamoto

The 60th Annual Meeting of the International Society of Electrochemistry (2009/8/16 -2009/8/21)

A high performance Si/C composite anode with carbon nanofiber for Li-ion batteries

Q. Si, K. Hanai, N. Imanishi, A. Hirano, Y. Takeda, O.Yamamoto

2nd International Conference on Advanced Lithium Battery for Automobile Applications（ABAA）(2009/11/25-2009/11/28)

A high performance Si/C composite anode with carbon nanofiber for Li-ion batteries

Q. Si, K. Hanai, N. Imanishi, A. Hirano, Y. Takeda, O.Yamamoto

第 50 回　電池討論会 （2009 年 11 月 30 日-2009 年 12 月 2 日）

CNF を用いたリチウム二次電池用新規 Si/C 複合負極材料の開発

斯　琴、 花井一真、 今西誠之、平野　敦、武田保雄、山本　治

粉体粉末冶金協会　平成 22 年度春季大会 （2010 年 5 月 25 日-2010 年 5 月 27 日）

カーボンナノファイバーを用いたリチウム二次電池用新規Si/C複合負極材料

斯　琴、 花井一真、 今西誠之、平野　敦、武田保雄、山本　治

15th International Meeting On Lithium Batteries (IMLB) (2010/6/27-2010/7/2)

A high performance Si/C composite anode for dry-polymer lithium secondary batteries

Q. Si, K. Hanai, N. Imanishi, A. Hirano, Y. Takeda, O.Yamamoto

第 51 回　電池討論会（2010 年 11 月 9 日-2010 年 11 月 11 日）

微粒子化とカーボン複合化によるSiO負極のサイクル特性の向上

斯　琴、 花井一真、 今西誠之、平野　敦、武田保雄、山本　治

3rd International Symposium on Advanced Plasma Science and its Applications for Nitrides and Nanomaterials (ISPlasma 2011) (2011/3/6-2011/3/9)

High Performance Si/Disordered Carbon with CNFs Composites for Lithium Ion Batteries

N. Imanishi, Q.Si, K. Hanai, A.Hirano, O.Yamamoto, Y.Takeda